IOPscience iopscience.iop.org

Home Search Collections Journals About Contact us My IOPscience

Surface-directed spinodal decomposition

This article has been downloaded from IOPscience. Please scroll down to see the full text article.

2005 J. Phys.: Condens. Matter 17 R101

(http://iopscience.iop.org/0953-8984/17/3/R01)

View the table of contents for this issue, or go to the journal homepage for more

Download details:
IP Address: 129.252.86.83
The article was downloaded on 27/05/2010 at 19:44

Please note that terms and conditions apply.

INSTITUTE OF PHYSICS PUBLISHING JOURNAL OF PHYSICS: CONDENSED MATTER

J. Phys.: Condens. Matter **17** (2005) R101–R142 doi:10.1088/0953-8984/17/3/R01

**TOPICAL REVIEW**

# Surface-directed spinodal decomposition

**Sanjay Puri**

School of Physical Sciences, Jawaharlal Nehru University, New Delhi-110067, India

Received 15 October 2004
Published 7 January 2005
Online at stacks.iop.org/JPhysCM/17/R101

**Abstract**

We review analytical and numerical results for *surface-directed spinodal decomposition* (SDSD), namely, the interplay of wetting kinetics and phase separation in a binary (AB) mixture in contact with a surface S which prefers one of the components (say, A). Depending on the relative strengths of the A–B, A–S and B–S interactions, the surface is either *partially wetted* or *completely wetted* by A in equilibrium. We discuss the theoretical framework for modelling SDSD, and review results obtained from both microscopic and coarse-grained models. We clarify the differences between diffusion-driven SDSD in solids, and SDSD in fluids, where velocity fields play an important role. Furthermore, we discuss the dependence of wetting-layer kinetics on the composition of the mixture. Some results are also presented for phase separation in a confined geometry, e.g., thin films. Finally, we discuss the problem of *surface-enrichment kinetics*, namely, the kinetics of enrichment of an attracting surface when the bulk mixture is stable. These nonequilibrium processes have important applications in the preparation of nanomaterials and multi-layered structures.

(Some figures in this article are in colour only in the electronic version)

## Contents



 © 2005 IOP Publishing Ltd Printed in the UK 

## 1. Introduction

Consider a binary (AB) mixture, which is homogeneous at high temperatures. This mixture becomes thermodynamically unstable if it is quenched below the coexistence curve. The subsequent evolution of the system is characterized by the emergence and growth of domains enriched in either component. This *far-from-equilibrium* phase-separation process is of great scientific and technological importance, and has attracted much research interest. It is prototypical of a large class of problems in the broad areas of *phase ordering dynamics* or *domain growth* or *coarsening kinetics*. The standard tools used to characterize pattern formation in phase ordering systems are (a) domain growth laws and (b) quantitative measures of the domain morphology like correlation functions, structure factors, domain-size distribution functions etc. There now exists a good understanding of domain growth in the bulk, and this has been reviewed by several authors [1–3].

Real experimental systems are confined in containers or have open surfaces, which often have a preferential attraction for one of the components of the mixture. This can have a drastic effect on the kinetics of phase separation, as we will discuss in this review article. In this context, it is important to clarify the equilibrium properties of an immiscible AB mixture in contact with a surface S. Let $\gamma_A$, $\gamma_B$ and $\sigma$ denote the surface tensions between AS, BS and AB, respectively. Without loss of generality, we assume that $\gamma_A < \gamma_B$, so that A is preferentially attracted to the surface. The contact angle between the AB interface and S is determined by Young's condition [4]:

$$\sigma \cos\theta = \gamma_B - \gamma_A. \tag{1}$$

For $\gamma_B - \gamma_A < \sigma$, both A and B are in contact with the surface, forming a *partially wet* (PW) morphology. However, equation (1) has no solution for $\gamma_B - \gamma_A > \sigma$. In this case, the B-rich phase is expelled from the surface and the component A covers the surface, forming a *completely wet* (CW) morphology. The equilibrium transitions between the PW and CW morphologies have been extensively studied [5–10]. Furthermore, the above discussion is easily generalized to include the effects of geometry and mixture composition [11].

Let us consider a generalization of the bulk phase separation problem. A homogeneous mixture is in contact with a surface with a preferential attraction for one of its components (say, A). The mixture is quenched deep below the coexistence curve, so that it undergoes phase separation in the bulk, and segregates into A-rich and B-rich domains. Simultaneously, the surface is wetted by the component A. The interplay of these two kinetic processes (i.e., phase

separation and wetting) is referred to as *surface-directed spinodal decomposition* (SDSD) or *surface-directed phase separation*, and has important technological applications.

We have a long-standing interest in SDSD, and this article reviews our understanding of this problem. We will also discuss the experimentally relevant problem of *surface-enrichment kinetics*, which refers to accretion of the preferred component from a stable (rather than unstable) mixture. Earlier reviews of analytical and numerical studies of SDSD are due to Puri and Frisch [12] and Binder [13]. The present review discusses current developments in this area in a pedagogical framework. A review of experimental studies of SDSD is due to Krausch [14]. A more recent review of experiments and technological applications has been written by Geoghegan and Krausch [15].

This review is organized as follows. In section 2, we provide a brief overview of experiments in this area. This is intended to motivate the subsequent discussion—a more detailed discussion of experiments is available in [14, 15]. In section 3, we discuss the modelling of SDSD at both the microscopic and coarse-grained levels. In section 4, we discuss analytical and numerical results for SDSD in a semi-infinite geometry. In section 5, we focus on phase separation in a confined geometry. Finally, in section 6, we turn to the problem of surface-enrichment kinetics. Section 7 concludes this paper with a summary and discussion.

## 2. Representative experimental results

### *2.1. Experiments on polymer mixtures*

The first experimental study of SDSD is due to Jones *et al* [16], who studied the segregation of mixtures of poly(ethylenepropylene) (PEP) and perdeuterated-PEP (dPEP). These mixtures had an open surface, which was preferentially wetted by d-PEP. Jones *et al* observed the formation of composition waves (or SDSD waves) with wavevectors normal to the surface, which propagated into the bulk, as shown in figure 1. These experiments did not provide quantitative results for the time-dependent evolution of the SDSD waves.

Krausch *et al* [17] improved on these experiments, studying a similar system but with better techniques. They focused on the time-dependence of the first 'zero'-crossing of the SDSD profiles (see figure 1 or 2), namely, the distance from the surface (say, $R_1(t)$ where $t$ is time) where the composition assumes its average value. Their results (see figure 2) showed that $R_1(t)$ obeyed the growth law $R_1(t) \sim t^{1/3}$, which is analogous to the Lifshitz–Slyozov (LS) law for diffusion-driven domain growth in the bulk [1]. The surface field was weak in the experiments of Krausch *et al*, and the surface was only partially wetted by droplets of the preferred phase.

A similar study is due to Bruder, Brenn and others [18, 19], who used critical mixtures of deuterated polystyrene (dPS) and partially brominated polystyrene ($PBr_xS$). They found that the preferred phase initially formed a plated layer at the surface, suggestive of a CW morphology. However, the CW morphology was metastable, and only grew out for a while before decomposing into a PW morphology. The layer thickness again obeyed the LS growth law, $R_1(t) \sim t^{1/3}$.

In a related experiment, Krausch *et al* [20] studied the evolution of an initial state consisting of a multi-layer of the coexisting phases of a polymer mixture (namely, dPS and $PBr_xS$) in contact with an unstable bulk. For early and intermediate times, they found that coarsening near the surface occurred by the dissolution of alternating layers of the initial structure. At late times, they again found results similar to those in [17–19].

It is of even greater interest to study the opposite limit of a strong surface field, which gives a CW morphology. In this case, there is rapid formation of a multi-layered structure at the surface, which consists of alternating layers of the preferred and non-preferred phases.

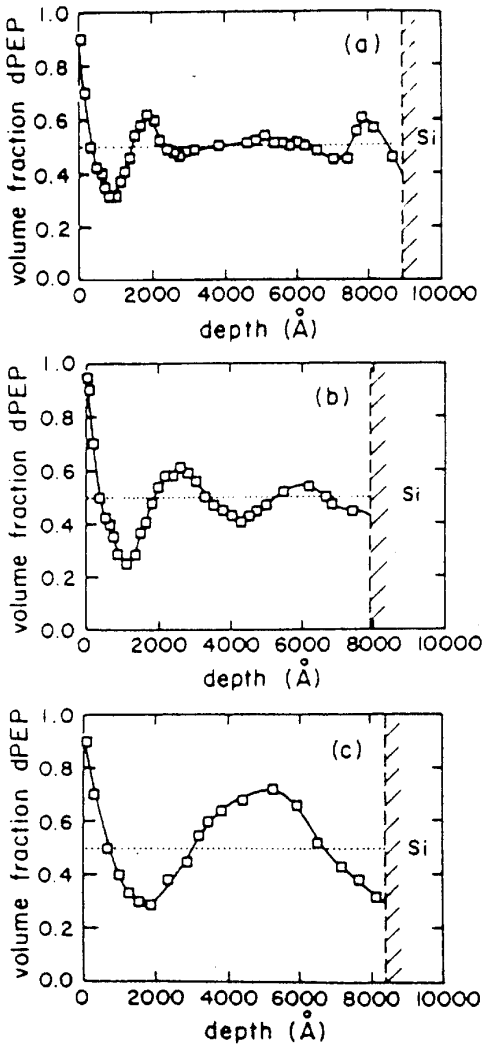


**Figure 1.** Evolution of laterally averaged profiles for an unstable polymer mixture (PEP and dPEP) in contact with an open surface which prefers dPEP [16]. The frames show the depth-dependence of the average density of dPEP at (a) 19 200 s, (b) 64 440 s and (c) 172 800 s after the quench. The average composition of the mixture is denoted by a dotted line.

For extended times, the growth of the wetting layer depends on the surface potential. The experiments of Geoghegan *et al* [21, 22] are relevant to this limit. These authors studied SDSD in blends of dPS and poly($\alpha$-methylstyrene) (P$\alpha$MS) for a variety of quench depths. They observed an LS growth of the wetting layer for deep quenches giving rise to a PW morphology, and much slower growth for shallow quenches corresponding to a CW surface morphology.

Recent interest has also focused on SDSD in other contexts. For example, various groups have studied SDSD on patterned substrates [23–25]. In these experiments, the surfaces are specially prepared (e.g., in a *checkerboard* or *striped* pattern) so that different regions are preferentially wetted by different components. This provides interesting possibilities for applications involving the preparation of nanomaterials and layered structures.

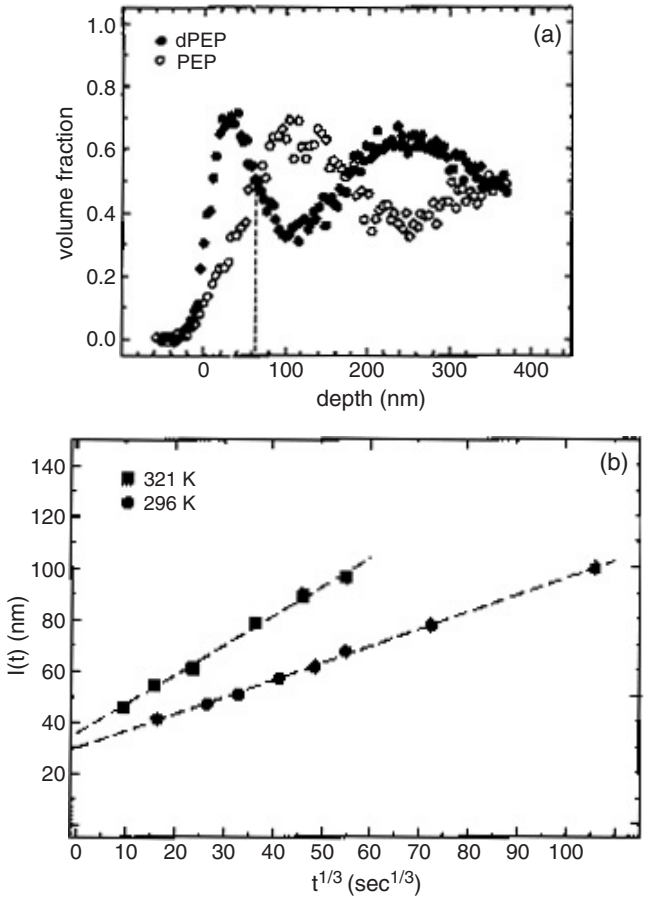


**Figure 2.** (a) Analogous to figure 1, but from the experiments of Krausch *et al* [17]. The laterally averaged profiles are shown for both polymers in the mixture (PEP and dPEP) at 14 400 s after the quench. To compare these profiles with those in figure 1, the pre-surface region of ∼20 nm should be discarded. (b) Plot of wetting-layer thickness versus $t^{1/3}$ for two different quench temperatures [17]. The dashed lines denote the best linear fits to the experimental data sets.

It is also experimentally relevant to study domain growth in the vicinity of the surface, and to clarify how it is affected by the growth of the wetting layer. We denote the length scales parallel and perpendicular to the surface as $L_{\parallel}(t)$ and $L_{\perp}(t)$ respectively. In the semi-infinite geometry, we expect $L_{\parallel}$, $L_{\perp} \to L(t)$ (the bulk domain size) at large distances from the surface. Again, we should distinguish between two different physical situations. In the PW case, where domains of both phases are in contact with the surface, it is reasonable to examine domain growth at the surface itself. On the other hand, in the CW case, where the surface is covered by a layer of the preferred phase, we consider domain growth outside the multi-layered structure. Straub *et al* [19] found that the lateral size of surface domains formed in the PW case obeys the LS growth law, $L_{\parallel}(t) \sim t^{1/3}$.

### *2.2. Experiments on fluid mixtures*

Let us next discuss some experiments on SDSD in binary fluid mixtures, where hydrodynamic velocity fields play an important role. Bulk phase separation is fluids is driven by advective

transport along domain boundaries, yielding faster growth in the asymptotic regime [26, 27]. An important set of experiments on SDSD in fluids is due to Wiltzius, Cumming and others [28–31], who observed a *fast mode* of surface domain growth in polymer and fluid mixtures. These authors found that the structure factor of the coarsening system exhibited two peaks, rather than the single peak usually seen in bulk spinodal decomposition. The position of one peak obeyed the appropriate bulk growth law, i.e., $L(t) \sim t$ for advective growth [26] or $L(t) \sim t^{1/3}$ for diffusive growth. However, the position of the other peak (located at larger length-scales) exhibited an anomalously fast growth law $L(t) \sim t^{\phi}$, with $\phi \sim 1.1$–$1.5$. These authors interpreted the fast growth as an early-time coating regime in which a droplet morphology evolves to one where the surface is completely layered. This interpretation has been supported by the molecular dynamics (MD) simulations of Ma *et al* [32, 33].

Guenoun *et al* [34] also studied the interplay of wetting and phase separation in fluid mixtures (cyclohexane and methanol) at critical concentrations. The time-regime they studied corresponds to a situation in which the surface is already coated with a layer of the preferred phase. They found that the wetting layer grew as $R_1(t) \sim t^{\phi}$, with $\phi \simeq 0.56$. Guenoun *et al* also reported that domain growth parallel to the surface was slower than bulk growth, and was characterized by a growth exponent $\phi \sim 0.5$–$0.7$.

Finally, Tanaka [35] has also conducted experiments on segregating polymer mixtures confined in capillaries with dimensionality $d = 1, 2$. Most of Tanaka's experiments were conducted on mixtures of polyvinylmethylether (PVME) and water, or oligomer mixtures. His primary focus was the interaction between phase separation and the wetting layer growing from the surface. In particular, he focused on the asymptotic regime, where hydrodynamic effects dominate the segregation dynamics. Tanaka found a strong dependence of the evolution morphology on the composition of the mixture. A recent review by Tanaka [36] summarizes results from his experiments, and provides useful scaling arguments for growth laws in fluid mixtures near a surface. We will reproduce some of these arguments in section 4.4.1.

### *2.3. Experimentally relevant issues*

Our survey of representative experimental results provides guidance to the relevant theoretical questions. It is appropriate to summarize the experimentally relevant issues which must be clarified by any reasonable theoretical framework for SDSD.

(1) The surface is rapidly enriched in the preferred component, and becomes the origin of SDSD waves which propagate into the bulk. What is the morphology and time-dependence of these waves? Does their nature depend on whether the surface exhibits a CW or PW morphology in equilibrium?
(2) What are the characteristics of domain growth in the vicinity of the wetting layer? For example, what are the growth laws characterizing segregation in the directions parallel and perpendicular to the surface?

The subsequent discussion primarily discusses the case where phase separation occurs via diffusion. At appropriate points, we will highlight the modifications which arise when hydrodynamic effects are incorporated.

## 3. Theoretical modelling

### *3.1. Models for bulk phase separation*

*3.1.1. Diffusive case.* The phase separation of binary (AB) mixtures can be modelled at both the microscopic and coarse-grained levels. At the microscopic level, a reasonable model is the

nearest-neighbour Ising Hamiltonian on a discrete lattice:

$$\mathcal{H} = -J \sum_{\langle ij \rangle} \sigma_i \sigma_j, \qquad \sigma_i = \pm 1, \tag{2}$$

where $J$ is the strength of the exchange coupling. For a site $i$, $\sigma_i = +1$ denotes an A atom and $\sigma_i = -1$ denotes a B atom. The subscript $\langle ij \rangle$ refers to a sum over nearest-neighbour pairs. The Ising model has no intrinsic dynamics, so we introduce stochastic kinetics by placing the system in contact with a heat bath. The ordering of a ferromagnet is modelled by *Glauber spin-flip* or *nonconserved* kinetics, where an arbitrary spin is flipped as $\sigma_i \to -\sigma_i$. On the other hand, the appropriate kinetics for the segregation of a binary mixture is *Kawasaki spin-exchange* or *conserved* kinetics, where a randomly chosen spin $\sigma_i$ is exchanged with a neighbour $\sigma_{L_i}$ as $\sigma_i \leftrightarrow \sigma_{L_i}$. The Kawasaki kinetic Ising model can be extended to include velocity fields, as in lattice-gas automata [37]. An alternative microscopic model for phase separation in fluids is obtained from MD simulations [38].

Next, let us discuss coarse-grained models of phase separation. For the diffusive case, a reasonable model is the Cahn–Hilliard–Cook (CHC) equation:

$$\begin{aligned} \frac{\partial}{\partial t}\psi(\vec{r},t) &= -\vec{\nabla}\cdot\vec{J}(\vec{r},t) \\ &= \vec{\nabla}\cdot[D\vec{\nabla}\mu(\vec{r},t) + \vec{\theta}(\vec{r},t)] \\ &= \vec{\nabla}\cdot\left[D\vec{\nabla}\left(\frac{\delta\mathcal{F}}{\delta\psi}\right) + \vec{\theta}(\vec{r},t)\right]. \end{aligned} \tag{3}$$

Here, $\psi(\vec{r},t)$ is the order parameter at space point $\vec{r}$ and time $t$. Equation (3) is also referred to as model B in the *critical dynamics* literature [39]. Typically, $\psi(\vec{r},t) = \rho_{\mathrm{A}}(\vec{r},t) - \rho_{\mathrm{B}}(\vec{r},t)$, where $\rho_{\mathrm{A}}$ and $\rho_{\mathrm{B}}$ denote the local densities of species A and B. In equation (3), the quantities $\vec{J}$, $D$ and $\mu$ denote the current, diffusion coefficient and chemical potential difference between A and B, respectively. The chemical potential is obtained as a functional derivative of the Helmholtz free energy, which is often taken to have the $\psi^4$-form:

$$\begin{aligned} \mathcal{F}[\psi] &= \mathcal{H} - TS \\ &\simeq \int \mathrm{d}\vec{r}\left[-\frac{1}{2}k_{\mathrm{B}}(T_{\mathrm{c}} - T)\psi^2 + \frac{k_{\mathrm{B}}T}{12}\psi^4 + \frac{J}{2}(\vec{\nabla}\psi)^2\right], \end{aligned} \tag{4}$$

where we have identified $\langle\sigma_i\rangle = \psi(\vec{r}_i)$ in equation (2) and Taylor-expanded various terms. Here, $T_{\mathrm{c}}$ denotes the critical temperature, and $T$ denotes the temperature. Finally, the Gaussian white noise term $\vec{\theta}(\vec{r},t)$ has zero average and obeys the fluctuation–dissipation relation:

$$\begin{aligned} &\overline{\vec{\theta}(\vec{r},t)} = 0, \\ &\overline{\theta_i(\vec{r'},t')\theta_j(\vec{r''},t'')} = 2Dk_{\mathrm{B}}T\delta_{ij}\delta(\vec{r'}-\vec{r''})\delta(t'-t''), \end{aligned} \tag{5}$$

where the bar denotes an ensemble average. Using a master-equation approach, the CHC equation can be motivated from the spin-exchange kinetic Ising model [40].

The diffusive phase separation of binary mixtures obeys the LS growth law, $L(t) \sim t^{1/3}$, which is obtained as follows. The chemical potential on the surface of a domain of size $L$ is $\mu \sim \sigma/L$, where $\sigma$ is the surface tension. The concentration current is obtained as $D|\vec{\nabla}\mu| \sim D\sigma/L^2$, where $D$ is the diffusion constant. Therefore, the domain size grows as $\mathrm{d}L/\mathrm{d}t \sim D\sigma/L^2$, or $L(t) \sim (D\sigma t)^{1/3}$.

*3.1.2. Incorporation of hydrodynamic effects.* We can incorporate hydrodynamic effects in the CHC equation by including a velocity field [39]. The resultant model for the order

parameter is

$$\frac{\partial}{\partial t}\psi(\vec{r},t) = \vec{\nabla}\cdot\left[D\vec{\nabla}\left(\frac{\delta\mathcal{F}}{\delta\psi}\right) - \psi\vec{v} + \vec{\theta}(\vec{r},t)\right], \tag{6}$$

where $\vec{v}(\vec{r},t)$ denotes the fluid velocity field which advectively transports the order parameter. We assume that the fluid is incompressible with constant density $\rho$. This imposes a constraint on the velocity field as $\vec{\nabla}\cdot\vec{v} = 0$.

The corresponding equation for the velocity field is the Navier–Stokes equation with an 'external' force term:

$$\frac{\partial}{\partial t}\vec{v}(\vec{r},t) = \eta\nabla^2\vec{v} - \left[\psi\vec{\nabla}\left(\frac{\delta\mathcal{F}}{\delta\psi}\right)\right]_\perp + [\vec{\zeta}(\vec{r},t)]_\perp, \tag{7}$$

where the pressure has been eliminated using the incompressibility condition, and $\eta$ is the viscosity. Furthermore, $[\vec{X}(\vec{r})]_\perp$ denotes the transverse part of the vector $\vec{X}(\vec{r})$. In momentum space, this is computed as

$$[\vec{X}(\vec{k})]_\perp = \vec{X}(\vec{k}) - \frac{\vec{k}\cdot\vec{X}(\vec{k})}{k^2}\vec{k}. \tag{8}$$

The Gaussian white noise in equation (6) satisfies the conditions in equation (5). The corresponding conditions for $\vec{\zeta}(\vec{r},t)$ in equation (7) are

$$\begin{aligned}&\overline{\vec{\zeta}(\vec{r},t)} = 0,\\ &\overline{\zeta_i(\vec{r'},t')\zeta_j(\vec{r''},t'')} = -2\eta k_{\mathrm{B}}T\delta_{ij}\nabla^2\delta(\vec{r'}-\vec{r''})\delta(t'-t'').\end{aligned} \tag{9}$$

Equations (6)–(9) are referred to as model H in the classification scheme of Hohenberg and Halperin [39]. Let us focus on the deterministic ($T = 0$) case. The relaxation of the velocity field is much faster than that of the order-parameter field. Thus, we set $\partial\vec{v}/\partial t = 0$ on the LHS of equation (7). The resultant equation is easily solved in Fourier space for $\vec{v}$ as

$$\begin{aligned}v_i(\vec{k},t) &= -T_{ij}(\vec{k})X_j(\vec{k},t)\\ &= -\frac{1}{\eta k^2}\left(\delta_{ij} - \frac{k_ik_j}{k^2}\right)X_j(\vec{k},t),\\ \vec{X}(\vec{k},t) &= \int \mathrm{d}\vec{r}\,\mathrm{e}^{\mathrm{i}\vec{k}\cdot\vec{r}}\psi\vec{\nabla}\left(\frac{\delta\mathcal{F}}{\delta\psi}\right).\end{aligned} \tag{10}$$

In equation (10), repeated indices are summed over and we have introduced the Oseen tensor $T_{ij}(\vec{k})$. In $d = 3$, the real-space Oseen tensor is

$$T_{ij}(\vec{r}) = \frac{1}{8\pi\eta r}\left(\delta_{ij} + \frac{r_ir_j}{r^2}\right). \tag{11}$$

Replacing the expression for the velocity in the deterministic version of the order-parameter equation, we obtain a closed evolution equation:

$$\frac{\partial}{\partial t}\psi(\vec{r},t) = \vec{\nabla}\cdot\left[D\vec{\nabla}\left(\frac{\delta\mathcal{F}}{\delta\psi}\right) + \psi\int \mathrm{d}\vec{r'}\,T_{ij}(\vec{r}-\vec{r'})X_j(\vec{r'},t)\right]. \tag{12}$$

Equation (12) is a good starting point for understanding the domain growth laws which govern coarsening in binary fluids. At early times, growth is diffusion limited, as in the case of binary alloys. However, there is a crossover to a hydrodynamic growth regime, where material is rapidly transported along domain boundaries by advection [26, 27]. The growth laws for

different regimes are summarized by Bray [1], and we quote the relevant results here:

$$L(t) \sim \begin{cases} (D\sigma t)^{1/3}, & L \ll (D\eta)^{1/2}, \quad \text{diffusive regime,} \\ \dfrac{\sigma t}{\eta}, & (D\eta)^{1/2} \ll L \ll \dfrac{\eta^2}{\rho\sigma}, \quad \text{viscous hydrodynamic regime,} \\ \left(\dfrac{\sigma}{\rho}\right)^{1/3} t^{2/3}, & \dfrac{\eta^2}{\rho\sigma} \ll L, \quad \text{inertial hydrodynamic regime.} \end{cases} \tag{13}$$

With this background, let us next consider the effect of surfaces on phase separation, both without and with hydrodynamics.

### *3.2. Early studies of SDSD*

An early study of SDSD is due to Xiong and Gong [41], who considered a semi-infinite system with a surface at $z = 0$. The order parameter obeys the CHC equation with the $\psi^4$ free-energy functional in equation (4):

$$\frac{\partial}{\partial t}\psi(\vec{\rho}, z, t) = \vec{\nabla} \cdot [\vec{\nabla}(-\psi + \psi^3 - \nabla^2\psi) + \vec{\theta}], \qquad z > 0, \tag{14}$$

where we have rescaled $\psi, \vec{r}, t$ into dimensionless units. (The nature of this rescaling will be discussed later.) We have introduced the notation $\vec{r} \equiv (\vec{\rho}, z)$, with $\vec{\rho}$ and $z$ denoting coordinates parallel and perpendicular to the surface, respectively. In this study, the surface gives rise to a delta-function (or short-ranged) potential, which only affects the boundary conditions. Xiong and Gong supplemented the CHC equation with a boundary condition at $z = 0$:

$$\left.\frac{\partial}{\partial z}\psi(\vec{\rho}, z, t)\right|_{z=0} = c\psi(\vec{\rho}, 0, t), \tag{15}$$

where $c$ measures the strength of the surface potential.

Following Langer *et al* [42], Xiong and Gong used this model as the basis of an approximate theory for the time-dependent structure factor in the surface layer. They found that phase separation in the boundary layer is faster than that in the bulk, but they did not quantify domain growth near the surface. Unfortunately, the Xiong–Gong study is open to criticism for two reasons. Firstly, their model is incomplete without a second boundary condition at the surface, which should be of the *no-flux* or *zero-current* type:

$$\left[\frac{\partial}{\partial z}(-\psi + \psi^3 - \nabla^2\psi) + \theta_z\right]_{z=0} = 0. \tag{16}$$

Secondly, the surface free energy used by Xiong and Gong to obtain equation (15) does not result in a preferential attraction of either of the components to the surface, and is unsuitable in the context of SDSD.

Jiang and Ebner [43] studied SDSD through Monte Carlo (MC) simulations of a semi-infinite Ising model with Kawasaki kinetics. They considered cases with both short-ranged and long-ranged (power-law) surface potentials. They found that the wetting layer thickness always obeyed the LS growth law, regardless of the potential. However, their results show a large degree of scatter and it is difficult to ascertain a conclusive growth exponent from their data.

The next relevant study is due to Ball and Essery [44], who modelled phase separation near surfaces using equations (14)–(16). As we have remarked earlier, the boundary condition in equation (15) does not lead to SDSD (for critical quenches) because the corresponding free energy does not discriminate between the two phases. For off-critical quenches, this model does exhibit symmetry breaking but in a somewhat artificial manner. Nevertheless,

the pioneering work of Ball and Essery motivated the initial experiments of Jones *et al* [16]. Furthermore, their study already recognized the effect of surface morphology on the evolution dynamics of the 'wetting' layer.

### *3.3. Hamiltonian for binary mixtures with surfaces*

A convenient starting point for modelling SDSD is the appropriate kinetic Ising model. This can be used as the basis for MC simulations. It can also be used to motivate coarse-grained models of SDSD.

Consider an AB mixture in contact with a planar surface S, located at $z = 0$. The mixture consists of $N_A$ A atoms and $N_B$ B atoms, with $N = N_A + N_B$. There are pair-wise interactions $-E_{ij}^{\alpha\beta}$ between species $\alpha$ and $\beta$ at sites $i$ and $j$. In terms of local concentration variables, $n_i^\alpha = 1$ if site $i$ is occupied by an $\alpha$ atom, and $n_i^\alpha = 0$ otherwise. The corresponding Hamiltonian is

$$\mathcal{H} = -\sum_{i>j=1}^{N} [E_{ij}^{AA} n_i^A n_j^A + E_{ij}^{BB} n_i^B n_j^B + E_{ij}^{AB}(n_i^A n_j^B + n_i^B n_j^A)] + \sum_{i=1}^{N} [V_A(\vec{r}_i) n_i^A + V_B(\vec{r}_i) n_i^B], \tag{17}$$

where lattice sites only exist in the positive half-space ($z \geqslant 0$). In equation (17), $V_A(\vec{r}_i)$ and $V_B(\vec{r}_i)$ are potentials on A and B atoms at site $i$ due to the hard wall at $z = 0$. In the case of a free surface (in contact with vacuum or air) at $z = 0$, it seems reasonable to set $V_A(\vec{r}_i) = V_B(\vec{r}_i) = 0$. However, this ignores the roughness of the interface between the mixture and the *vapour phase* at $z < 0$. For solids above their roughening transition temperature $T_R$ [45, 46] (and for fluid mixtures, where the fluid–gas interface is always rough), this assumption is only reasonable on length scales much larger than the scale of atomic roughness. Furthermore, we expect that the pair-wise interactions $-E_{ij}^{\alpha\beta}$ depend not only on the relative distance $|\vec{r}_i - \vec{r}_j|$, but also on $\vec{r}_i, \vec{r}_j$ separately. For example, different interactions occur if both sites $i$, $j$ are in the surface layer (labelled as $i_z = 0$) [7, 47].

As usual, we only consider the case with nearest-neighbour interactions. Furthermore, the interactions are taken to be independent of the sites $i$ and $j$, except when both of these lie in the surface layer. The potential usually depends only on the distance from the surface. It is experimentally relevant to consider both short-ranged potentials ($V(z) \sim \delta(z)$ or $V(z) \sim \exp(-z/z_0)$, where $z_0$ is the characteristic decay length) and long-ranged power-law potentials ($V(z) \sim z^{-n}$). We stress that there are significant physical differences between wetting by short-ranged and long-ranged potentials [10].

We introduce Ising variables through the transformation $\sigma_i = 2n_i^A - 1 = 1 - 2n_i^B$. The resultant Ising Hamiltonian is

$$\mathcal{H} = -\sum_{\langle ij \rangle} J_{ij}\sigma_i\sigma_j - H\sum_{i=1}^{N}\sigma_i - H_1\sum_{i_z=0}\sigma_i + \sum_{i_z\neq 0} V(z_i)\sigma_i + \mathcal{H}_0, \tag{18}$$

where $\mathcal{H}_0$ is a constant which only affects the energy scale. The pair-wise exchange interaction $J_{ij}$ is

$$J_{ij} = \begin{cases} J = \dfrac{E^{AA} + E^{BB} - 2E^{AB}}{4}, & i_z \text{ or } j_z \neq 0, \\ J_s = \dfrac{E_s^{AA} + E_s^{BB} - 2E_s^{AB}}{4}, & i_z,\, j_z = 0. \end{cases} \tag{19}$$

Here, the subscript s denotes the pair-wise interaction in the surface layer. The bulk 'magnetic field' $H$ is

$$H = \frac{q}{4}(E^{AA} - E^{BB}), \tag{20}$$

where $q$ is the coordination number of a site. For sites in the surface layer, the magnetic field (for a cubic lattice) is

$$H + H_1 = \frac{q-2}{4}(E_s^{AA} - E_s^{BB}) + \left(\frac{E^{AA} - E^{BB}}{4}\right) - \left[\frac{V_A(0) - V_B(0)}{2}\right]. \quad (21)$$

Finally, the potential is identified as

$$V(z_i) = \frac{V_A(z_i) - V_B(z_i)}{2}. \quad (22)$$

The potential contribution at the surface has been absorbed into the definition of $H_1$. For the case of a delta-function potential, which only acts in the surface layer, the potential term $V(z_i)$ is absent in equation (18).

It is important to note that a non-zero surface field $H_1$ arises even when $V_A = V_B = 0$, and interactions are unchanged at the surface, i.e., $E_s^{AA} = E^{AA}$ and $E_s^{BB} = E^{BB}$, provided $E^{AA} - E^{BB} \neq 0$. This is a consequence of the missing neighbours of sites in the surface layer. This field vanishes if we consider the symmetric case $E^{AA} = E^{BB}$, but this has little physical relevance for real binary mixtures. Therefore, a surface field typically appears whenever a surface is introduced.

The bulk field in equation (18) is irrelevant because we work in a fixed-concentration ensemble with $\sum_i \sigma_i = N_A - N_B$. However, the surface field $H_1$ and the potential term remain as parameters in the problem. These terms are responsible for both surface enrichment and wetting phenomena in mixtures [7–10]. The generalization of the Hamiltonian in equation (18) to any other geometry is obvious. For example, in a $d = 2$ capillary of thickness $D$, the RHS of equation (18) contains additional terms arising from the introduction of a surface at $z = D$. The framework for characterization of equilibrium critical phenomena for binary mixtures at surfaces has been discussed earlier by various authors [7–10, 12]. We will not replicate this discussion here, but rather refer the interested reader to these earlier works.

We conclude this discussion by formulating the coarse-grained free-energy functional corresponding to the Hamiltonian in equation (18). As usual, we introduce the space-dependent order parameter $\langle \sigma_i \rangle = \psi(\vec{r}_i)$, and Taylor-expand around the point $\vec{r}_i$ to obtain

$$\begin{aligned}\mathcal{F}[\psi] \simeq \int \mathrm{d}\vec{r} \left[-\frac{1}{2}k_B(T_c - T)\psi^2 + \frac{k_B T}{12}\psi^4 + \frac{J}{2}(\vec{\nabla}\psi)^2 + V(z)\psi\right] \\ + \int \mathrm{d}\vec{\rho} \left\{-\tfrac{1}{2}[(q-2)J_s + J - k_B T]\psi(\vec{\rho}, 0)^2 - H_1\psi(\vec{\rho}, 0) \right. \\ \left. + \frac{J_s}{2}[\vec{\nabla}_\parallel \psi(\vec{\rho}, 0)]^2 - \frac{J}{2}\psi(\vec{\rho}, 0)\frac{\partial\psi}{\partial z}\bigg|_{z=0}\right\} \\ \equiv \mathcal{F}_b + \mathcal{F}_s. \end{aligned} \quad (23)$$

The term $\mathcal{F}_b$ is the bulk free energy in equation (4) supplemented by a surface potential term, and $\mathcal{F}_s$ is the surface contribution. Here, the different value of the exchange interaction in the surface layer has been explicitly accounted for. The term $\partial\psi/\partial z|_{z=0}$ in $\mathcal{F}_s$ appears because of the missing neighbours for $z < 0$. The expansion which results in equation (23) is only justifiable near criticality, where the order-parameter amplitude is small. However, we will also use this free energy for parameter values far from criticality. The justification for this lies in the ability of the resultant model to describe experimental phenomenology. The appropriate minimal model for description of surface critical phenomena has been discussed extensively in the literature [10].

### *3.4. Dynamical models for SDSD*

A reasonable microscopic model for SDSD is obtained by associating Kawasaki kinetics with the Ising Hamiltonian in equation (18). There have been MC studies of such kinetic Ising models, and we will discuss these shortly. However, the coarse-grained counterpart of the kinetic Ising model is expected to be more amenable to theoretical analysis. In early work, Binder and Frisch [48] used the master equation for the kinetic Ising model to obtain a phenomenological model for SDSD with a delta-function surface potential. The Binder–Frisch model consisted of the Cahn–Hilliard (CH) equation (i.e., deterministic version of the CHC equation) in the bulk supplemented by two boundary conditions representing the surface. One of these was modified by Puri and Binder [49], who explicitly incorporated a no-flux boundary condition into the model. The Puri–Binder model was the first successful coarse-grained model for SDSD. Let us derive it directly from the free-energy functional in equation (23), as was done for the CHC equation (3).

The bulk order-parameter equation is obtained from equation (3) with $\mathcal{F}[\psi]$ from equation (23). The resultant CHC equation is then

$$\frac{\partial}{\partial t}\psi(\vec{r},t) = \vec{\nabla}\cdot\left\{D\vec{\nabla}\left[-k_{\mathrm{B}}(T_{\mathrm{c}}-T)\psi + \frac{k_{\mathrm{B}}T}{3}\psi^3 - J\nabla^2\psi + V(z)\right] + \vec{\theta}\right\}. \tag{24}$$

Now, the order parameter rapidly relaxes to its equilibrium value at the surface, and is not a conserved quantity. Therefore, we assume a relaxational (model A [39]) kinetics for the order parameter at the surface. This yields (ignoring thermal fluctuations) the first boundary condition:

$$\begin{aligned}\lambda^{-1}\frac{\partial}{\partial t}\psi(\vec{\rho},0,t) &= -\frac{\delta\mathcal{F}}{\delta\psi(\vec{\rho},0,t)} \\ &= [(q-2)J_{\mathrm{s}} + J - k_{\mathrm{B}}T]\psi + H_1 + \frac{J}{2}\frac{\partial\psi}{\partial z}\bigg|_{z=0},\end{aligned} \tag{25}$$

where $\lambda^{-1}$ sets the timescale. The lateral-diffusion term has been neglected in the second expression of equation (25) because the order parameter rapidly saturates to its equilibrium value at the surface. The second boundary condition is the no-flux condition at $z = 0$:

$$0 = \left\{D\frac{\partial}{\partial z}\left[-k_{\mathrm{B}}(T_{\mathrm{c}}-T)\psi + \frac{k_{\mathrm{B}}T}{3}\psi^3 - J\nabla^2\psi + V(z)\right] + \theta_z\right\}_{z=0}. \tag{26}$$

It is convenient to rescale this model into dimensionless units. As we are interested in unstable mixtures, we consider the case with $T < T_{\mathrm{c}}$ and introduce the following rescaled quantities:

$$\begin{aligned}&\psi' = \frac{\psi}{\psi_0}, \qquad \psi_0 = \sqrt{3\left(\frac{T_{\mathrm{c}}}{T}-1\right)}, \\ &\vec{r}' = \frac{\vec{r}}{\xi_{\mathrm{b}}}, \qquad \xi_{\mathrm{b}} = \left[\frac{q}{2}\left(1-\frac{T}{T_{\mathrm{c}}}\right)\right]^{-1/2}, \\ &t' = \frac{t}{t_0}, \qquad t_0 = \frac{\xi_{\mathrm{b}}^2}{Dk_{\mathrm{B}}(T_{\mathrm{c}}-T)}, \\ &\vec{\theta}' = \frac{t_0}{\xi_{\mathrm{b}}\psi_0}\vec{\theta}, \\ &V'(z') = \frac{1}{\psi_0 k_{\mathrm{B}}(T_{\mathrm{c}}-T)}V(\xi_{\mathrm{b}}z').\end{aligned} \tag{27}$$

Here, $\xi_b$ is the bulk correlation length. This yields the dimensionless CHC equation (dropping the primes):

$$\frac{\partial}{\partial t}\psi(\vec{r},t) = \vec{\nabla}\cdot\left\{\vec{\nabla}\left[-\psi+\psi^3-\frac{1}{2}\nabla^2\psi+V(z)\right]+\vec{\theta}\right\}, \qquad z>0, \tag{28}$$

where

$$\begin{aligned}&\overline{\vec{\theta}(\vec{r},t)} = 0,\\ &\overline{\theta_i(\vec{r'},t')\theta_j(\vec{r''},t'')} = 2\epsilon\delta_{ij}\delta(\vec{r'}-\vec{r''})\delta(t'-t''),\end{aligned} \tag{29}$$

with the noise amplitude

$$\epsilon = \frac{1}{3}\left(\frac{T_c}{T}-1\right)^{-2}\xi_b^{-d}. \tag{30}$$

The corresponding dimensionless boundary conditions are as follows:

$$\tau_0\frac{\partial}{\partial t}\psi(\vec{\rho},0,t) = h_1+g\psi+\gamma\left.\frac{\partial\psi}{\partial z}\right|_{z=0}, \tag{31}$$

$$0 = \left\{\frac{\partial}{\partial z}\left[-\psi+\psi^3-\frac{1}{2}\nabla^2\psi+V(z)\right]+\theta_z\right\}_{z=0}, \tag{32}$$

where $\tau_0 = \lambda^{-1}D/\xi_b^2$. The other parameters in the boundary conditions are as follows:

$$h_1 = \frac{H_1}{\psi_0 k_B(T_c-T)}, \tag{33}$$

$$g = \frac{(q-2)J_s+J-k_BT}{k_B(T_c-T)}, \tag{34}$$

$$\gamma = \frac{J}{2\xi_b k_B(T_c-T)}. \tag{35}$$

Equation (31) rapidly relaxes the surface value of the order parameter to its equilibrium value, and will be replaced by its static version ($\tau_0 = 0$) subsequently. The surface potential and the parameters $\epsilon, h_1, g, \gamma$ determine the equilibrium phase diagram of the surface [12, 50, 51].

In this context, let us study the static solutions of the $T = 0$ version of equations (28), (31) and (32). These are obtained by setting $\partial\psi/\partial t = 0$. Ignoring lateral fluctuations, the $z$-dependent static solution $\psi_s(z)$ is obtained as the solution of

$$\psi_s - {\psi_s}^3 + \frac{1}{2}\frac{d^2\psi_s}{dz^2} - V(z) = 0, \tag{36}$$

with the boundary condition

$$\frac{h_1}{\gamma}+\frac{g}{\gamma}\psi_s(0)+\left.\frac{d\psi_s}{dz}\right|_{z=0} = 0. \tag{37}$$

Puri and Binder [51] have obtained solutions of equations (36) and (37) for the case of a short-ranged surface potential. The corresponding phase diagram in the $(g/\gamma, h_1/\gamma)$-plane is shown in figure 3. As expected, it is symmetric under $h_1 \to -h_1$. The phase diagram exhibits lines of both first-order and second-order transitions, meeting in a tricritical point. Note that $\xi_b \to \infty$ and $\psi_0 \to 0$ as $T \to T_c^-$. In this limit, $h_1/\gamma \sim \xi_b^2 \to \infty$ for $h_1 > 0$. Furthermore, $g/\gamma \sim \xi_b \to \infty$ for $g > 0$, and $-\infty$ for $g < 0$. Thus, as the system approaches the critical point, it is deep in the wetting region of the phase diagram [5]. In a typical experiment, one is

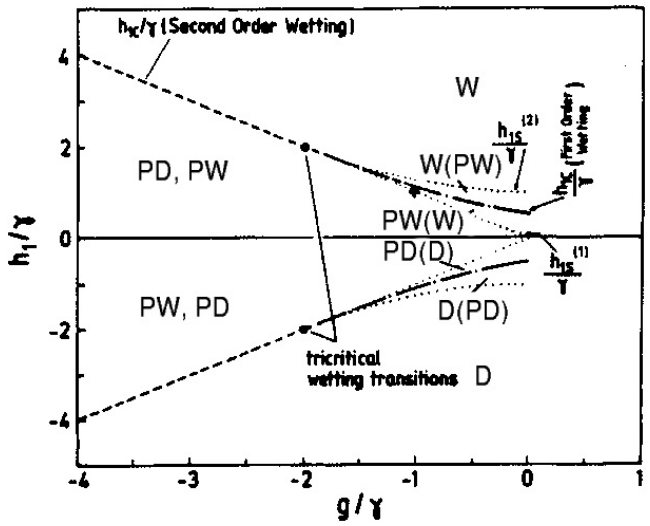


**Figure 3.** Phase diagram in the $(g/\gamma, h_1/\gamma)$-plane for the case of a delta-function surface potential. The states are labelled as W (wet) or dry (D), and PW (partially wet) or PD (partially dry). The metastable states, if any, are specified in brackets. The dashed lines denote lines of second-order transitions, and have equations $h_1/\gamma = \mp g/\gamma,\ g/\gamma < -2$ in the upper and lower half-planes. The dot–dashed lines denote lines of first-order transitions and are obtained from a graphical construction. The second-order and first-order lines meet at tricritical points. The dotted lines are the spinodals associated with the first-order phase transitions. In the upper half-plane, their equations are $h_1/\gamma = -g/\gamma,\ g/\gamma > -2$ (lower spinodal) and $h_1/\gamma = 1 + g^2/(4\gamma^2),\ g/\gamma > -2$ (upper spinodal). Analogous equations determine the spinodals in the lower half-plane.

interested in spinodal decomposition and wetting far from the bulk critical point. Therefore, we shall use the present model for parameter choices of $h_1/\gamma, g/\gamma \sim \mathrm{O}(1)$ as well.

The dynamical model described above is appropriate for a semi-infinite geometry. The extension to a thin-film (or any other) geometry is straightforward—the boundary conditions in equations (25) and (26) have to be implemented on all surfaces with appropriate parameters. There are novel effects in phase separation in confined geometries due to the interaction of SDSD waves arising from different boundaries [11, 52–54].

The modelling described above has been in the context of diffusive dynamics. However, many of the experiments on SDSD involve fluid mixtures (see section 2.2), where hydrodynamic effects play an important role. Again, one could consider microscopic models, e.g., MD simulations of mixtures near surfaces. There have been a number of such studies (which are discussed later), and they provide valuable information about the ongoing kinetic processes. Alternatively, one can study coarse-grained models like model H at a surface. The boundary conditions on the order-parameter field are similar to those described earlier. However, these must now be supplemented with boundary conditions on the velocity field, e.g., the velocity vanishes at the surface. There have been a few studies of model H at surfaces, and these will also be discussed shortly.

Finally, we mention the work of Diehl and Janssen [55], who have studied the *critical dynamics* (rather than *far-from-equilibrium dynamics*) of model B at a surface. These authors have used symmetry considerations to classify possible boundary conditions. Diehl and Janssen have also examined the physical implications of different boundary conditions for critical dynamics at a surface.

### 3.5. Characterization of SDSD

As stated earlier, the characterization of SDSD involves understanding (1) the growth kinetics and morphology of the wetting layer, and (2) domain growth in the vicinity of the wetting layer. We already have a good understanding of bulk phase-separation kinetics, and this will serve as a useful reference point.

The morphology of the wetting layer is quantified via laterally averaged order-parameter profiles as in figures 1 and 2. Recall that the SDSD profiles decay to the homogeneous value of the order parameter in the bulk. The wetting-layer kinetics is characterized by the growth laws governing the zero-crossings of the laterally averaged profiles.

In the bulk, domain growth is characterized by equal-time correlation functions and structure factors. These are time dependent since one focuses on far-from-equilibrium systems. For domain growth near surfaces, it is appropriate to define layer-wise correlation functions, which depend on the distance from the surface. The relevant quantities are as follows:

(a) the $z$-dependent correlation function,

$$C_{\parallel}(\vec{\rho}_1 - \vec{\rho}_2, z, t) = \langle \psi(\vec{\rho}_1, z, t)\psi(\vec{\rho}_2, z, t)\rangle - \langle \psi(\vec{\rho}_1, z, t)\rangle\langle \psi(\vec{\rho}_2, z, t)\rangle, \tag{38}$$

and

(b) its Fourier transform, the $z$-dependent structure factor:

$$S_{\parallel}(\vec{k}_{\parallel}, z, t) = \int \mathrm{d}\vec{\rho}\, \exp(\mathrm{i}\vec{k}_{\parallel} \cdot \vec{\rho}) C_{\parallel}(\vec{\rho}, z, t). \tag{39}$$

The angular brackets in equation (38) denote an average over independent realizations of the evolution. In equation (39), $\vec{k}_{\parallel}$ denotes the wavevector component which is parallel to the surface.

We can also consider the more general correlation function:

$$C(\vec{\rho}_1 - \vec{\rho}_2, z_1, z_2, t) = \langle \psi(\vec{\rho}_1, z_1, t)\psi(\vec{\rho}_2, z_2, t)\rangle - \langle \psi(\vec{\rho}_1, z_1, t)\rangle\langle \psi(\vec{\rho}_2, z_2, t)\rangle. \tag{40}$$

Notice that there is no translational invariance in the $z$-direction because of the surface located at $z = 0$. We can identify $C_{\parallel}(\vec{\rho}_1 - \vec{\rho}_2, z, t) = C(\vec{\rho}_1 - \vec{\rho}_2, z, z, t)$. The counterpart of this generalized correlation function in Fourier space is defined as follows:

$$S(\vec{k}, z, t) = \int \mathrm{d}\vec{\rho} \int_0^{\infty} \mathrm{d}z'\, \exp[\mathrm{i}\vec{k}_{\parallel} \cdot \vec{\rho} + \mathrm{i}k_{\perp}(z' - z)] C(\vec{\rho}, z', z, t), \tag{41}$$

where $k_{\perp}$ denotes the wavevector component which is perpendicular to the surface. The surface excess of the scattering intensity of the system is then

$$S_{\mathrm{s}}(\vec{k}, t) = \int_0^{\infty} \mathrm{d}z\, [S(\vec{k}, z, t) - S_{\mathrm{b}}(\vec{k}, t)], \tag{42}$$

where $S_{\mathrm{b}}(\vec{k}, t)$ is the bulk structure factor.

In studies of bulk phase separation, length scales are defined from the decay of the correlation function or as inverse moments of the structure factor [56]. Here, one considers the characteristic length $L_{\parallel}(z, t)$, describing the growth of correlations parallel to the surface at a distance $z$ from the surface. This is defined as the distance over which the appropriate correlation function decays to (say) half its maximum value, i.e.,

$$C_{\parallel}(L_{\parallel}, z, t) = \frac{C_{\parallel}(0, z, t)}{2}. \tag{43}$$

A perpendicular length scale $L_{\perp}(z, t)$ can be defined similarly. In the semi-infinite geometry,

$$L_{\parallel}(z, t), L_{\perp}(z, t) \to L(t), \qquad \text{as } z \to \infty, \tag{44}$$

where $L(t)$ is the bulk length scale.

## 4. Results for surface-directed spinodal decomposition

### *4.1. Early-time behaviour*

The nonlinear model in equations (28)–(32) is not analytically tractable. However, the growth of fluctuations in the early-time regime can be understood by solving a linearized version of this model. This is obtained by setting $\psi = \psi_0 + \psi'$, where $\psi_0$ is the average order parameter of the system and $\psi'$ denotes small fluctuations around $\psi_0$. The linear model in $\psi'$ is as follows (dropping the primes):

$$\frac{\partial}{\partial t}\psi(\vec{r},t) = \vec{\nabla}\cdot\left\{\vec{\nabla}\left[(3\psi_0^2-1)\psi - \frac{1}{2}\nabla^2\psi + V(z)\right] + \vec{\theta}\right\}, \qquad z > 0, \tag{45}$$

with the boundary conditions

$$0 = \left(\frac{h_1}{\gamma} + \frac{g}{\gamma}\psi_0\right) + \frac{g}{\gamma}\psi + \left.\frac{\partial\psi}{\partial z}\right|_{z=0}, \tag{46}$$

$$0 = \left\{\frac{\partial}{\partial z}\left[(3\psi_0^2-1)\psi - \frac{1}{2}\nabla^2\psi + V(z)\right] + \theta_z\right\}_{z=0}, \tag{47}$$

where we have set $\tau_0 = 0$. The solution of the bulk linearized model with $V(z) = 0$ is straightforward. However, in the present case, one has to account for the surface potential and two boundary conditions at the surface.

Binder and Frisch [48] solved the linear problem for a delta-function surface potential, and a stable bulk with $T > T_c$. They studied the equilibration of a homogeneous initial condition, and showed that the resultant surface-enrichment profile has a minimum whose distance from the wall grows as $t^{1/2}$. Two remarks are in order here. Firstly, the kinetics of surface enrichment for a stable mixture is also an experimentally relevant problem [57, 58], and will be discussed in section 6. Secondly, the solution of the linear problem is similar for both surface enrichment and SDSD, though the physics is quite different. The solution of the surface-enrichment problem is reasonable for all times. On the other hand, the solution of the linear SDSD problem is only valid for early times. At later times, the growing fluctuations must be saturated by nonlinearities in the dynamical equations. Nevertheless, an early-time theory of SDSD is useful to predict the selected wavelengths of surface-directed profiles. Frisch *et al* [59] studied the linear regime of SDSD, and found that the initial evolution replicated the damped concentration profiles seen in figure 1.

In this context, another interesting study is due to Fischer *et al* [60]. Recall that the boundary condition in equation (31) ignored surface diffusion, because the field homogenizes the order parameter at the surface. Fischer *et al* undertook an analysis of linear SDSD in the absence of a surface field but with surface diffusion, and found that novel instabilities arise for certain parameter ranges.

### *4.2. Dynamics of wetting and phase separation*

*4.2.1. Wetting for critical mixtures* ($\psi_0 = 0$). Next, let us discuss the kinetics of wetting-layer growth, and phase separation adjacent to the wetting layer. The discussion follows that of Puri and Binder [61] and Puri *et al* [62], who have studied SDSD using the model in equations (28)–(32) for a wide range of mixture compositions and power-law potentials:

$$V(z) = \begin{cases} -V_0, & z \leqslant 1, \\ -\dfrac{V_0}{z^n}, & z > 1. \end{cases} \tag{48}$$

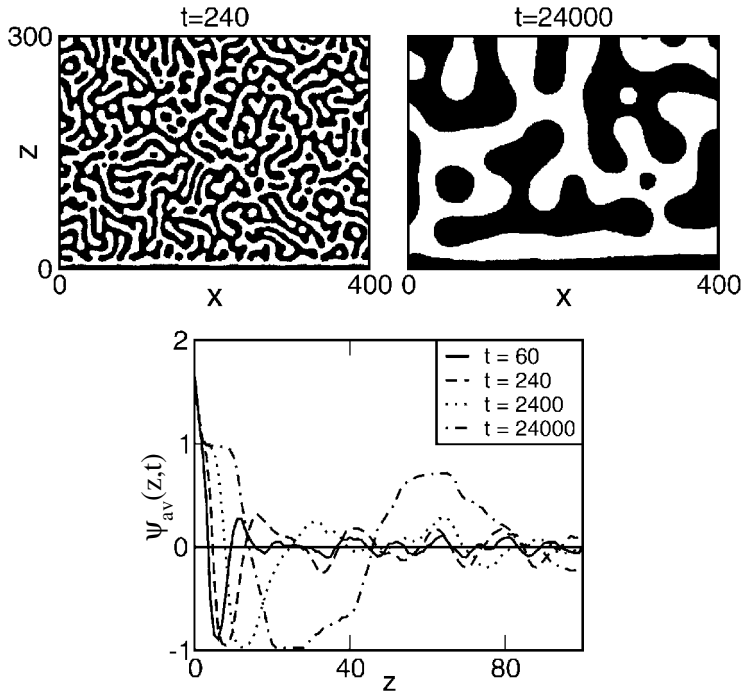


**Figure 4.** Evolution of an unstable AB mixture from a homogeneous initial condition with a critical composition ($\psi_0 = 0$). The snapshots in the upper frames are obtained from an Euler-discretized version of equations (28)–(32) on a $d = 2$ square lattice of size $L_x \times L_z$ (with $L_x = 400$ and $L_z = 300$). The mesh sizes in space and time are $\Delta x = 1$ and $\Delta t = 0.03$. The surface is located at $z = 0$ and attracts A (with $\psi > 0$, marked in black) through the power-law potential in equation (48) with $n = 4$ and $V_0 = h_1 = 0.8$. The other parameter values are $g = -0.4$ and $\gamma = 0.4$, corresponding to complete wetting in equilibrium. The noise amplitude is $\epsilon = 0.041$, which corresponds to a deep quench with $T \simeq 0.22T_c$ from equation (30). The lower frame shows laterally averaged profiles for the evolution at dimensionless times $t = 60, 240, 2400$ and 2400. The solid line is drawn at $\psi_{av} = \psi_0$, and denotes the average order parameter. Notice the two-step wetting profile at the surface.

Here, the lower cut-off is chosen to avoid the power-law singularity at $z = 0$. Power-law potentials are common in the context of surface–molecule interactions, e.g., $n = \kappa - d$, with $\kappa = 6$ and 7 corresponding to cases with non-retarded and retarded van der Waals' interactions, respectively [63, 64]. The short-ranged case is recovered in the limit $n \to \infty$. For simplicity, we will consider the case with $E^{AA} = E^{BB}$ and $E_s^{AA} = E_s^{BB}$ in equation (21). In that case, the dimensionless surface field is $h_1 = -V(0) = V_0$.

In figure 4, we show the evolution of a critical binary mixture (i.e., average order parameter $\psi_0 = 0$) from a homogeneous initial condition. The simulation details and parameter values are provided in the figure caption. The surface (at $z = 0$) is completely wetted by the component A (marked in black), and shows a multi-layered morphology, i.e., wetting layer followed by depletion layer, etc. This morphology is time-dependent and propagates into the bulk, as seen from the laterally averaged profiles shown in the lower frame. These are obtained by averaging $\psi(x, z, t)$ along the $x$-direction for a typical evolution, and further averaging over 200 independent runs. This procedure is the numerical counterpart of the lateral averaging which yielded the density–depth profiles in figures 1 and 2. The averaging procedure gives $\psi_{av}(z, t) \simeq \psi_0 = 0$ in the bulk, where the segregation profiles are randomly oriented. However,

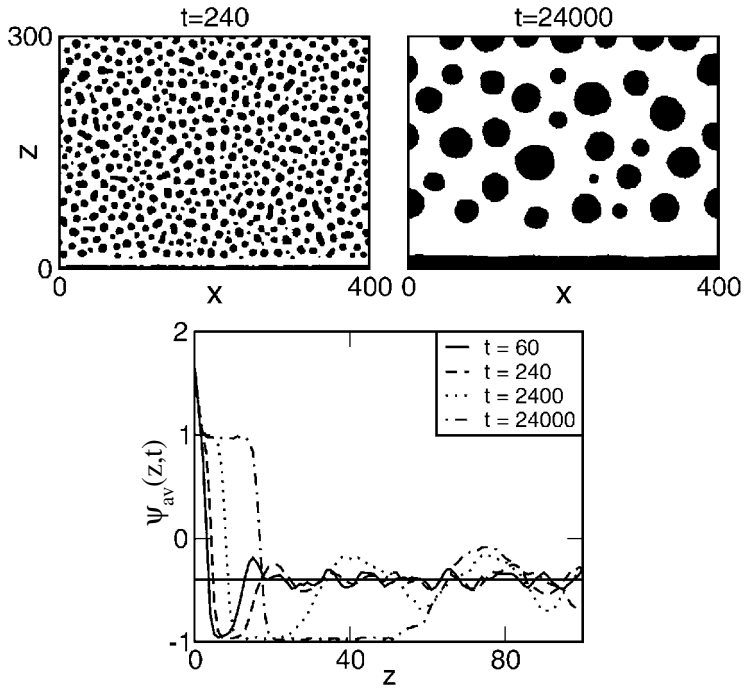


**Figure 5.** Analogous to figure 4, but for the case where the minority component wets the surface, with $\psi_0 = -0.4$.

a systematic behaviour is seen at the surface. The wetting profiles are characterized by the zero-crossings of $\psi_{\rm av}(z,t) - \psi_0$, and $R_1(t)$ and $R_2(t)$ denote the first and second zeros, respectively. A phenomenological theory for these quantities will be formulated shortly.

Puri *et al* [49, 62] have studied domain growth adjacent to the wetting layer for a critical quench and a variety of surface potentials. They characterize domain growth using $z$-dependent correlation functions and structure factors, as defined in section 3.5. Their studies suggest the following picture. Domains near the wetting layer are characterized by two length scales $L_\parallel(z,t)$, $L_\perp(z,t) \sim t^{1/3}$, with $L_\parallel > L_\perp$ (see figure 4). The length scale parallel to the surface is larger because of the orientational effect of the multi-layered morphology at the surface. However, the enhancement is only in the prefactor of the growth law. These length scales cross over to diffusive growth [$L_\parallel(z,t) \sim t^{1/2}$] as the domains are absorbed into the wetting layer which propagates into the bulk. In this review, we will primarily focus on the evolution of the SDSD profiles. For detailed results on anisotropic domain growth adjacent to the wetting layer, we refer the interested reader to the papers of Puri *et al* [49, 62].

*4.2.2. Wetting by the minority component* ($\psi_0 < 0$). Next, consider the effect of asymmetric composition on the growth kinetics of the wetting layer. First, we consider the case where the wetting component is the minority component in the mixture.

Figure 5 shows the evolution from a homogeneous initial condition with $\psi_0 = -0.4$, corresponding to a mixture with 30% A (the preferred component) and 70% B. In the snapshots shown in the top frames, the bulk (large $z$) is characterized by a droplet morphology, which is usual for off-critical phase separation [56, 65]. As in figure 4, there is a wetting layer of the preferred component at the surface, which is followed by a depletion layer. The surface

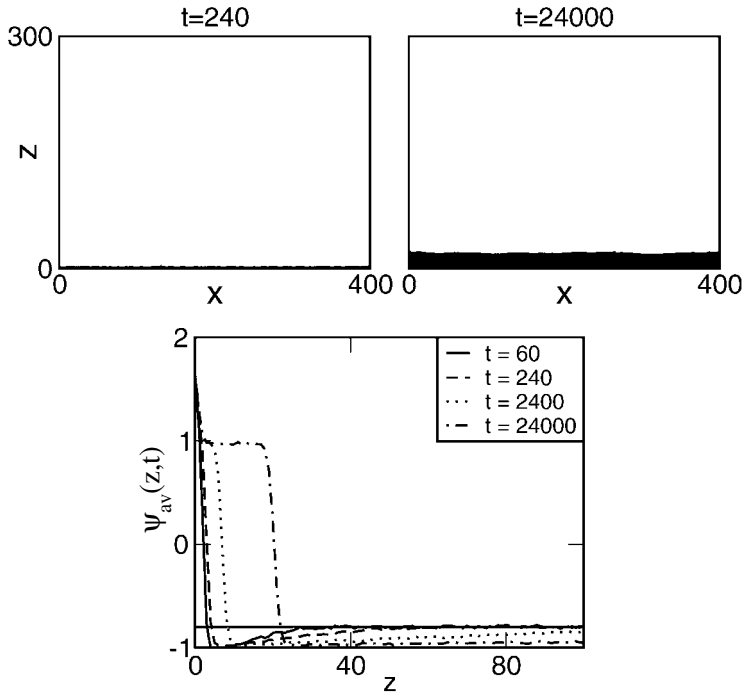


**Figure 6.** Analogous to figure 4, but for $\psi_0 = -0.8$.

morphology is clarified by the laterally averaged profiles shown in the bottom frame. At comparable times, the thickness of the wetting and depletion layers is larger than in figure 4.

Next, consider the evolution of an extremely off-critical case ($\psi_0 = -0.8$ or 10% A and 90% B) in figure 6. In this case, the thermal fluctuations are not sufficient to nucleate an A-rich droplet on the timescale of the simulation. Thus, there is no bulk phase separation, but there is a rapid growth of the wetting layer at the surface. The behaviour is qualitatively different from that for $\psi_0 = 0.0, -0.4$, due to the absence of bulk phase separation. The lower frame of figure 6 shows that the A-rich wetting layer is followed by a layer which is moderately depleted in A, and extends deep into the bulk.

Let us first understand the time-dependence of the wetting profiles seen in figures 4 and 5, where the bulk undergoes phase separation. We denote the thickness of the depletion layer as $h(t) = R_2(t) - R_1(t)$. Consider the typical snapshots in figures 4 and 5. There are two contributions to the current which drives the growth of the wetting layer.

(1) The surface-potential gradient drives A to the wetting layer with a current $-\mathrm{d}V/\mathrm{d}z|_{z=R_1}$.
(2) The intrinsic chemical potential due to local curvature is higher on the curved surface of bulk A-rich domains (of length scale $L$) than on the flat wetting layer (of length scale $\infty$). This difference is estimated as $\sigma/L$, and the corresponding current contribution at the wetting layer is $-\sigma/(Lh)$.

Thus the A-current in the $z$-direction is obtained by adding these two contributions as follows:

$$J_z \simeq -\left.\frac{\mathrm{d}V(z)}{\mathrm{d}z}\right|_{z=R_1} - \frac{\sigma}{Lh}. \tag{49}$$

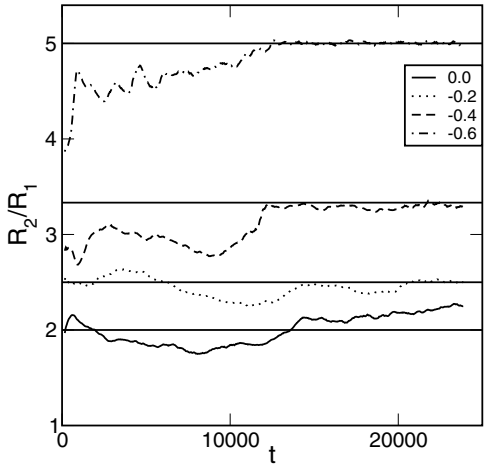


**Figure 7.** Plot of $R_2/R_1$ versus $t$ for $\psi_0 = 0.0, -0.2, -0.4, -0.6$. We define $R_1(t)$ as the first $z$-value at which $\psi_{\rm av}(z,t)$ crosses $\psi_0$, and $R_2(t)$ as the second $z$-value at which $\psi_{\rm av}(z,t)$ crosses $\psi_0$. The horizontal lines are drawn at $R_2/R_1 = 2/(1+\psi_0)$.

To estimate $h(t)$, assume that the wetting and depletion layers have an overall composition of $\psi_0$. This yields the relations

$$R_2(t) \simeq \frac{2}{1+\psi_0} R_1(t), \qquad h(t) \simeq \frac{1-\psi_0}{1+\psi_0} R_1(t). \tag{50}$$

The validity of the scaling assumption in equation (50) is demonstrated in figure 7, where we plot $R_2/R_1$ versus $t$ for $\psi_0 = 0, -0.2, -0.4$ and $-0.6$.

Using the power-law form of the potential from equation (48), and $h(t)$ from equations (50), equation (49) yields [61]

$$\frac{{\rm d}R_1}{{\rm d}t} = -J_z \simeq \frac{nh_1}{{R_1}^{n+1}} + \frac{\sigma}{LR_1}\left(\frac{1+\psi_0}{1-\psi_0}\right). \tag{51}$$

The bulk length scale obeys the LS growth law $L(t) = f(\psi_0)(\sigma t)^{1/3}$, where the function $f(\psi_0)$ is known analytically for $|\psi_0| \to 1$ [1], but only numerically for other values of $\psi_0$ [56]. The first term on the RHS of equation (51) is dominant at early times (for $n > 1$) and the second term is dominant at late times. This yields the growth regimes as

$$R_1(t) \sim \begin{cases} (h_1 t)^{1/(n+2)}, & t \ll t_{\rm c}, \\ \sqrt{\dfrac{(1+\psi_0)}{f(\psi_0)(1-\psi_0)}}(\sigma t)^{1/3}, & t \gg t_{\rm c}. \end{cases} \tag{52}$$

The crossover time $t_{\rm c}$ is obtained by equating the early-time and late-time length scales as (for $n > 1$)

$$t_{\rm c} \sim h_1^{3/(n-1)} \sigma^{-(n+2)/(n-1)} \left[\frac{f(\psi_0)(1-\psi_0)}{(1+\psi_0)}\right]^{3(n+2)/[2(n-1)]}. \tag{53}$$

Clearly, the crossover between the potential-dependent regime and the universal regime ($R_1 \sim t^{1/3}$) can be extremely delayed, depending on the various system parameters and mixture composition. This clarifies the reason for the diverse growth exponents reported by various experiments and numerical simulations. Figure 8(a) plots $\ln[R_1(t)]$ versus $\ln t$ for

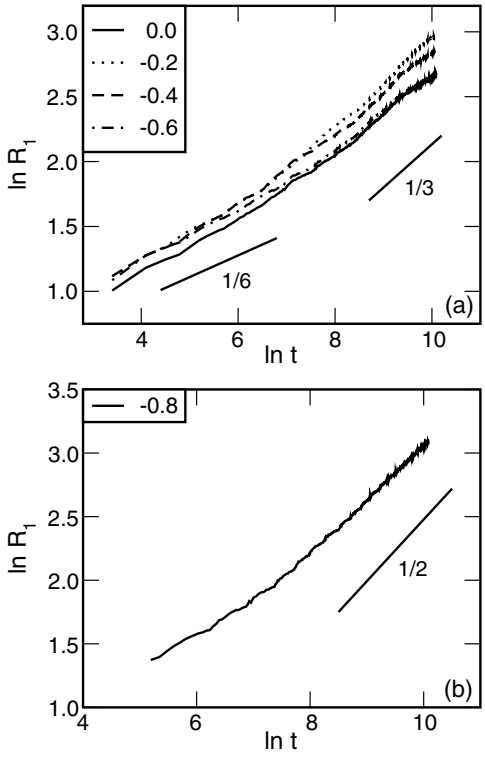


**Figure 8.** (a) Time-dependence of the wetting-layer thickness, ln $R_1$ versus ln $t$, for mixtures with different composition: $\psi_0 = 0.0, -0.2, -0.4, -0.6$. The straight lines have slopes $1/6$ and $1/3$, respectively. The exponent $\phi = 1/6$ corresponds to potential-dependent growth for the case of nonretarded van der Waals' interactions with $n = 4$ in $d = 2$. (b) Plot of ln $R_1$ versus ln $t$ for an extremely off-critical composition with $\psi_0 = -0.8$. The straight line has a slope of 1/2.

$\psi_0 = 0.0, -0.2, -0.4, -0.6$ and illustrates this crossover behaviour. Figure 8(b) shows the corresponding data for $\psi_0 = -0.8$, which will be discussed shortly.

Before proceeding, let us make some comments regarding the case of a critical quench with $\psi_0 = 0$. As both components are present in equal proportions, the bulk is bicontinuous and has surfaces with both positive and negative curvatures. This suggests that the second term on the RHS of equation (51) should be replaced by its average value, which changes sign as $\psi_0$ goes through zero. This would result in a divergence of the crossover time in equation (53) as $\psi_0 \to 0$. However, figure 8(a) does not show this because the $\psi_0 = 0$ evolution morphology is also characterized by A-rich droplets in the region subsequent to the depletion layer (see the snapshot at $t = 240$ in figure 4). These droplets arise because of the flow of A to the wetting layer through the depletion layer.

Let us briefly comment on the cases of the power-law potential with $n = 1$, and the short-ranged potential $V(z) = -V_0 \exp(-z/z_0)$. For $V(z) \sim -z^{-1}$, both terms on the RHS of equation (51) are comparable for all times and the resultant growth law is the LS law, $R_1(t) \sim t^{1/3}$. On the other hand, the short-ranged potential yields a logarithmic early-time growth, $R_1(t) \sim z_0 \ln(h_1 t/z_0^2)$, which rapidly crosses over to the universal LS growth law. However, thermal fluctuations may interfere with the observation of the logarithmic growth regime [66].

Finally, consider the case of highly off-critical quenches ($\psi_0 \ll 0$), where there is no bulk phase separation as in figure 6. Here, there are no droplets in the bulk to feed the wetting layer. Thus, the bulk chemical potential is the uniform value $\mu_0 = {\psi_0}^3 - \psi_0$. The corresponding current to the wetting layer is $-\mu_0/h$, where $h(t)$ is now the scale on which the order parameter exponentially saturates to its bulk value (see the lower frame of figure 6). We neglect lateral fluctuations and assume a simple form for $\psi(z,t)$ as follows:

$$\psi(z,t) \simeq \begin{cases} 1, & z < R_1(t), \\ \psi_0 - B_0 \mathrm{e}^{-(z-R_1)/h}, & z > R_1(t), \end{cases} \tag{54}$$

where $B_0$ is a parameter. This form will be justified when we discuss the kinetics of surface enrichment in section 6. The composition constraint then yields

$$h(t) \simeq \frac{(1-\psi_0)}{B_0} R_1(t). \tag{55}$$

Thus, equation (51) is modified as

$$\begin{aligned} \frac{\mathrm{d}R_1}{\mathrm{d}t} &\simeq \frac{nh_1}{{R_1}^{n+1}} + \frac{\mu_0 B_0}{1-\psi_0}\frac{1}{R_1} \\ &= \frac{nh_1}{{R_1}^{n+1}} + \frac{|\psi_0|(1+\psi_0)B_0}{R_1}. \end{aligned} \tag{56}$$

The corresponding growth regimes in this case are (for any value of $n$)

$$R_1(t) \sim \begin{cases} (h_1 t)^{1/(n+2)}, & t \ll t_\mathrm{c}, \\ [|\psi_0|(1+\psi_0)B_0]^{1/2} t^{1/2}, & t \gg t_\mathrm{c}. \end{cases} \tag{57}$$

The crossover from potential-dependent growth to a universal diffusive growth law occurs at the crossover time

$$t_\mathrm{c} \sim h_1^{2/n} [|\psi_0|(1+\psi_0)B_0]^{-(n+2)/n}. \tag{58}$$

Figure 8(b) plots $\ln[R_1(t)]$ versus $\ln t$ for $\psi_0 = -0.8$, illustrating the asymptotically diffusive growth of the wetting layer. For a short-ranged surface potential, the initial growth regime is logarithmic, as before.

*4.2.3. Wetting by the majority component* ($\psi_0 > 0$). Finally, we focus on off-critical compositions with $\psi_0 > 0$, so that the majority component wets the surface. Figure 9 shows the evolution of a homogeneous initial condition with $\psi_0 = 0.4$. Now, the droplets are of the non-wetting component. A thin wetting layer is formed and grows very slowly, as seen in the lower frame of figure 9. The depletion layer that forms adjacent to the wetting layer is hardly apparent in this case.

At first, it seems counter-intuitive that the wetting layer grows so slowly when the majority component wets the surface. Essentially, the bulk droplets now compete with (rather than feed) the wetting layer for the preferred component A, as the intrinsic chemical potential for A is lower on the surface of the drops. Thus, only the first term on the RHS of equation (51) is operational, and wetting-layer growth is driven only by the surface potential with $R_1(t) \sim t^{1/(n+2)}$. As a matter of fact, the wetting-layer growth is even slower because the intrinsic chemical-potential gradient actually drives A into the bulk [61]. Similar considerations apply for other values of $\psi_0 > 0$, when the bulk undergoes phase separation.

The extremely off-critical case (with $\psi_0 \gg 0$) is analogous to enrichment kinetics seen for $T > T_\mathrm{c}$, if there is no nucleation of droplets over extended timescales. If droplets are nucleated, the scenario described for $\psi_0 = 0.4$ is applicable again. In section 6, we will discuss surface enrichment at length.

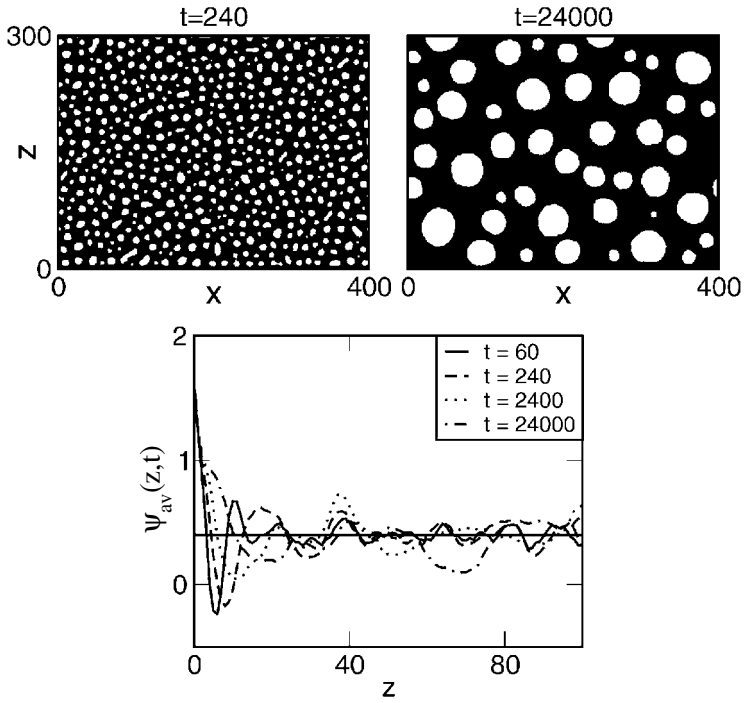


**Figure 9.** Analogous to figure 4, but for the case where the majority component wets the surface, with $\psi_0 = 0.4$.

### *4.3. Other relevant studies of SDSD*

The discussion so far has followed the work of Puri *et al* [61, 62]. Now, we discuss other important studies of this problem. In early work, Brown and Chakrabarti [67] undertook a Langevin simulation of SDSD in $d = 2$ with both short-ranged and long-ranged surface fields. Their model was similar to that described in section 3.4, but the parameter values gave rise to a PW surface morphology. Brown and Chakrabarti found that the surface layer thickness obeyed the LS growth law, $R_1(t) \sim t^{1/3}$. They also showed that length scales perpendicular and parallel to the surface were consistent with the LS growth law, but $L_\parallel > L_\perp$. This is in conformity with the results described in section 4.2. Brown *et al* [68] also reported an interesting study of *surface-induced nucleation*, where they considered a metastable mixture in contact with a surface. The flow of the preferred component to the surface facilitated the nucleation of droplets adjacent to the wetting layer. This corresponds to the case discussed in section 4.2.3, with $\psi_0 > 1/\sqrt{3}$, the mean-field spinodal. Brown *et al* found that the wetting-layer thickness showed very slow growth, as explained in section 4.2.3.

Brown and Chakrabarti also studied SDSD in block copolymer melts in both semi-infinite and film geometries [69]. Following Oono and Shiwa [70], they modelled block copolymers by the $\psi^4$ free-energy functional in conjunction with a long-ranged interaction term. For bulk phase separation, it is known that coarsening block copolymers freeze into a meso-structure, whose length scale depends inversely on the strength of the long-ranged interaction potential [70, 71]. Analogous effects occur for SDSD in block copolymers, and some of these are discussed by Brown and Chakrabarti [69].

A comprehensive *cell dynamical system* (CDS) [56] study of SDSD in $d = 2, 3$ was reported by Marko [72], who investigated cases with both short-ranged and long-ranged surface

potentials. Marko carefully studied domain growth morphologies and the laterally averaged profiles in both PW and CW cases. For the PW morphology, he found results consistent with those of Brown and Chakrabarti [67] for the growth of wetting layers. On the other hand, in the CW case, he found a drastic slowing down of wetting layer growth. This is consistent with the potential-dependent growth regime discussed in section 4.2.2.

There have also been studies of microscopic models for SDSD. For example, Sagui *et al* [73] reported a $d = 3$ MC study of the spin-exchange Ising model with a short-ranged surface field. They studied situations with both zero and non-zero surface fields. Recall that phase separation can occur in the surface layer, even if the bulk is stable, by an appropriate choice of interactions. For the case of a stable bulk and unstable surface, Sagui *et al* found that lateral growth in the surface layer was consistent with the Lifshitz–Allen–Cahn (LAC) growth law which characterizes nonconserved dynamics, namely, $L_{\|}(t) \sim t^{1/2}$. For the case where both the bulk and surface are unstable, Sagui *et al* found that the growth exponent in the surface layer ranged from $\phi = 1/2 \rightarrow 1/3$, depending on the quench depth. The lower exponents correspond to deeper quenches.

Finally, there have also been Langevin simulations of SDSD on patterned substrates by Karim *et al* [23], in conjunction with their experiments on polymer blends. These Langevin studies suggested ways of controlling the phase-separation morphology near the surface. Lee *et al* [74] have also adapted the models described in section 3.4 to study the effect of immobile obstacles with non-rectangular shapes (e.g., spheres or cylinders) on spinodal decomposition.

### *4.4. Role of hydrodynamic effects*

Next, let us consider the role of hydrodynamic effects in SDSD. At the outset, we stress that domain connectivity is crucial in enabling advective transport of the order parameter. For off-critical fluid mixtures with isolated droplets of the minority component, SDSD is driven by diffusive transport as described above. For near-critical fluid mixtures, we expect novel features due to the presence of hydrodynamic effects.

*4.4.1. Arguments for growth exponents.* In section 3.1.2, we saw that bulk binary fluids coarsen faster than binary solids, due to advective transport of the order parameter by the velocity field. This results in the growth law $L(t) \sim (\sigma/\eta)t$ in the *viscous hydrodynamic* regime, where $\sigma$ is the surface tension and $\eta$ is the fluid viscosity (see equation (13)).

Here, we derive the growth exponents characterizing SDSD in binary fluids. In many experiments on SDSD, the surface is initially coated by the preferred component, regardless of whether the equilibrium morphology is PW or CW. The dynamics of coating has been discussed by Tanaka [35, 36]. The bulk tubes are in contact with the surface, and the pressure gradient between the bulk and surface results in a flux $\sim(\sigma/\eta)L^2$, where $L$ is the tube size. Under strong wetting conditions, this flux results in the lateral spreading of a layer droplet of size $L_s(t)$, whose growth (in $d = 3$) is then determined by $\mathrm{d}L_s^2/\mathrm{d}t \sim (\sigma/\eta)L^2$. Using the Siggia growth law, $L(t) \sim (\sigma/\eta)t$, one obtains the surface growth law $L_s(t) \sim (\sigma/\eta)^{3/2}t^{3/2}$, which is consistent with the experimental observations of a fast mode by Wiltzius, Cumming and others [28, 29]. The above arguments also yield the crossover time to complete coating as $t_c \sim \eta/\sigma$.

Next, we consider the dynamics of wetting layer growth. If one neglects the early potential-dependent regime, we can describe the growth as follows. The wetting layer grows due to the flux of material from the tube into the surface layer. For the hydrodynamic problem, this yields $S(\mathrm{d}R_1/\mathrm{d}t) \sim (\sigma/\eta)L^2 \times (S/L^2)$, where $S$ is the surface area and $S/L^2$ is the number of tubes. Thus, $R_1(t) \sim (\sigma/\eta)t$ for the wetting-layer dynamics also. However, this result is

at variance with the experiments of Guenoun *et al* [34], who observed much slower growth of the wetting layer. This discrepancy could be due to transient growth laws dependent upon the surface potential, as discussed in section 4.2.

*4.4.2. Numerical studies.* An early numerical study of SDSD in fluid mixtures is due to Ma *et al* [32, 33], who performed MD simulations of binary (AB) fluids confined in a thin film. They considered two different cases: (a) both A and B are equally repulsed by the walls, and (b) one of the walls has a preferential attraction for A. In the first case, Ma *et al* studied density-correlation functions in the parallel direction, and found that these exhibited reasonable dynamical scaling, except when the capillary was too thin, i.e., comparable to the molecular diameter. The associated length scale was $L_{\|} \sim t^{\phi}$ with $\phi \simeq 0.54$, which they claimed to be consistent with the experiments of Guenoun *et al* [34]. However, the two physical situations are considerably different so a comparison is inappropriate. A more credible explanation is that the MD simulation in (a) is analogous to phase separation in $d = 2$ fluids, which is characterized by the exponent $\phi = 2/3$ [38]. The second case of Ma *et al* is relevant to the SDSD problem. In this case, they observe a *fast mode* in the surface layer, but with an exponential rather than power-law growth.

Another early MD study is due to Zhang and Chakrabarti [75], who considered a fluid mixture confined in a $d = 1$ capillary. These authors focused on equilibrium rather than dynamical issues, and studied the conditions under which capsule/tube (or CW) and plug (or PW) morphologies are obtained for the phase-separated mixture in the capillary. These morphologies are discussed in detail in section 5.2.

As stated earlier, a reasonable coarse-grained model for SDSD in a binary fluid is model H, supplemented with appropriate boundary conditions. Chen and Chakrabarti [76] have studied SDSD (in $d = 2$) by numerically solving model H in a semi-infinite geometry. They consider a surface with a long-ranged potential and impose *no-slip* conditions on the velocity field at the surface. Their primary result is that the wetting-layer growth crosses over from $R_1(t) \sim t^{1/3}$ (characteristic of diffusive growth in $d > 1$) to $R_1(t) \sim t^{2/3}$ (characteristic of hydrodynamic growth in $d = 2$ [38]). This crossover occurs because domains of the preferred component drain rapidly into the surface layer.

Another study of model H (in $d = 3$) in a semi-infinite geometry is due to Tanaka and Araki [77, 36]. They find that the wetting-layer thickness initially grows as $R_1(t) \sim t^{1/3}$, and then crosses over to the hydrodynamic regime with $R_1(t) \sim t$. Tanaka and Araki also find that the oscillatory profile of SDSD waves is destroyed more rapidly in the hydrodynamic case than in the diffusive case. These authors also studied growth laws in the layers parallel to the surface. In the vicinity of the surface, they found a faster growth than $L_{\|} \sim t$, the usual bulk law. However, they could not associate an unambiguous exponent with this faster growth. Furthermore, the time-regime of this 'fast mode' is considerably later than the formation of the CW layer. This suggests that the fast growth observed by Tanaka and Araki may be associated with the anisotropic growth ($L_{\|} > L_{\perp}$) of domains due to orientational effects of the wetting layer, rather than the fast mode of [28–31]. As discussed earlier, this fast mode is associated with the coating dynamics which results in the formation of a wetting layer.

A recent MD study by Toxvaerd [78] investigated a critical AB mixture phase-separating in a thin film. The particles interact with each other and the walls via Lennard-Jones potentials. Toxvaerd focused on the morphologies which arise for different wall-types, e.g., one wall attracts A whereas the other wall attracts B; both walls attract A and B equally, etc. In all cases, he finds that the system evolves into a layered morphology, with the layer being parallel to the surface walls. These 'layered states' are metastable configurations which evolve slowly due to the low dimensionality of the system.

In recent work, Bastea *et al* [79] used meso-scale models to study SDSD in $d = 3$ fluids. These models are at an intermediate level between the microscopic and coarse-grained models discussed so far, and were first introduced by Bastea and Lebowitz [80] to study bulk domain growth. They consist of coupled Vlasov–Boltzmann equations for a mixture (AB) of hard spheres with equal diameters and a long-range repulsion between the two components. This mesoscopic representation has the advantage that the relevant conservation laws are automatically satisfied, and it also provides a rigorous route to a macroscopic description. At the computational level, the method introduced in [80], i.e., coupling of the *direct simulation Monte Carlo* algorithm for close-range collisions [81] and the *grid-weighting method* for the long-range repulsions [82], permits the study of much bigger systems than those used in MD simulations.

In the corresponding study of SDSD [79], one of the components of the binary mixture (say, A) interacts with the surface (located at $z = 0$) through the power-law potential $V(z)$ in equation (48) with $n = 3$. Recall that this corresponds to the case of nonretarded van der Waals' interactions in $d = 3$. The wall is diffusive [83], i.e., particles hitting the wall are absorbed and re-emitted isotropically with a velocity drawn from a Maxwellian distribution with the surface temperature $T_s$. The simulations were done on critical mixtures at $T = 0.6T_c$, $T_s = T$, where $T_c$ is the bulk mean-field critical temperature of the system. The parameter varied was the strength of the surface–particle interaction, $V_0$.

The simulations of Bastea *et al* clarified the wetting-layer kinetics in both the PW and CW cases. In figure 10, we show evolution pictures and laterally averaged profiles for the PW case. In figure 11, we show the corresponding results for the CW case. Bastea *et al* found that the wetting-layer growth was consistent with the Siggia law ($R_1(t) \sim t$) in the PW case, but substantially slower (consistent with the LS law for diffusive growth, $R_1(t) \sim t^{1/3}$) in the CW case.

Finally, Kuksenok *et al* [84, 85] have used lattice-Boltzmann and CDS models to study AB fluids flowing on a patterned substrate. In their simulations, the substrate is decorated with a chequerboard pattern, with different patches preferring A or B. Kuksenok *et al* studied the interplay between phase separation and the competing drive for alignment with the surface pattern.

## 5. Phase separation in a confined geometry

So far, we have primarily described modelling and results for phase separation in semi-infinite systems. As stated earlier, the modelling of phase separation in confined geometries is a straightforward generalization. Thus, for a thin film of thickness $D$, we impose the boundary conditions in equations (25) and (26) at $z = D$ with an appropriate surface potential [52].

There exists a good understanding of the equilibrium properties of confined mixtures [11, 86–90]. In general, the equilibrium morphologies depend on the confinement geometry and surface potentials. A detailed discussion of the possible morphologies for a symmetric thin film is presented in section 5.2. The dynamical evolution of confined mixtures is much more complex due to the interaction of SDSD waves originating from different surfaces. However, there have been relatively few investigations of these problems. Let us discuss two recent works on SDSD in confined systems.

### *5.1. SDSD in cylindrical samples of steel mixtures*

In section 2, we had reviewed representative experimental results for SDSD in polymers and fluids. Recently, Aichmayer *et al* [91] have reported the first experimental observation

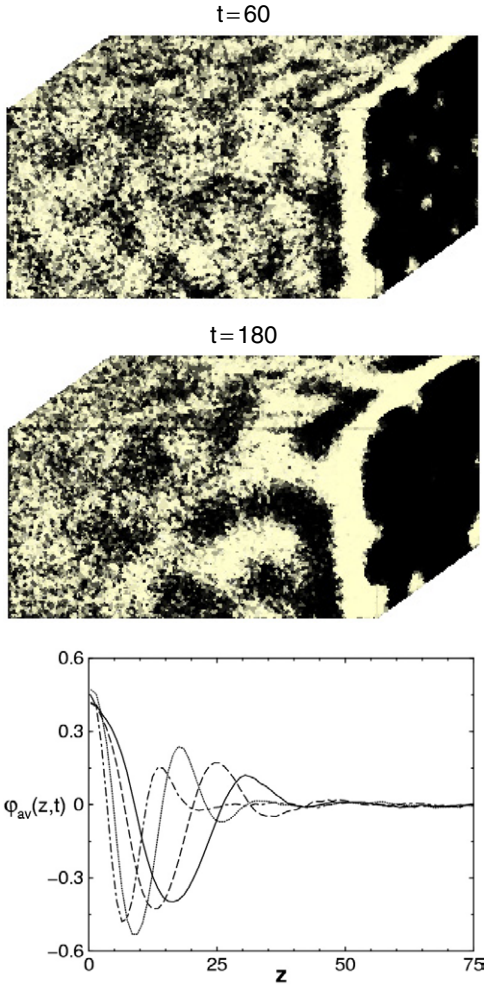


**Figure 10.** SDSD in an unstable binary fluid with critical composition [79]. The snapshots in the upper frames were obtained from simulations of meso-scale models based on the coupled Vlasov–Boltzmann equations for a mixture of hard spheres. The surface (located on the right) is partially wetted by the preferred component, which is marked in black. The lower frame shows laterally averaged profiles for the evolution at times $t = 50$, 100, 200 and 275 (from left to right).

of SDSD in solid mixtures of ferrite ($\delta$, bcc) and austenite ($\gamma$, fcc) stainless steels. These mixtures were prepared as cylindrical samples with diameter 10 mm, and were quenched into the two-phase ($\delta + \gamma$) region of the phase diagram. The $\delta$-phase is preferentially driven to the surface due to (a) the atmosphere around the samples and (b) the presence of long-ranged strain fields. Figure 12 shows the evolution of the unstable mixture. An enriched layer of the ferrite phase forms at the surface, followed by a depletion layer and then the bulk region, analogous to figures 4 and 5. The SDSD profiles propagate into the bulk, resulting in a macroscopic segregated state (see the snapshot at $t = 48$ h), which is dictated by the composition of the mixture.

Aichmayer *et al* also undertook Langevin simulations of the dimensionless SDSD model in equations (28)–(32) in a cylindrical geometry. In polar coordinates $\vec{r} = (r, \phi)$, the appropriate

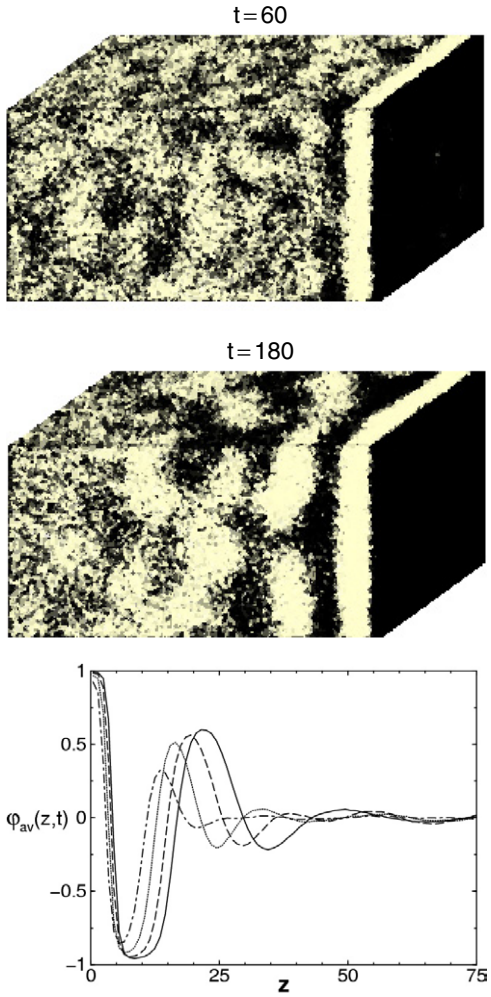


**Figure 11.** Analogous to figure 10, but for the case of a completely wet surface morphology.

model is

$$\frac{\partial}{\partial t}\psi(r,\phi,t) = -\vec{\nabla}\cdot\vec{J} = \vec{\nabla}\cdot\left\{\left[-\psi+\psi^3-\frac{1}{2}\nabla^2\psi+V(r)\right]+\vec{\theta}\right\}. \tag{59}$$

In this case, the surface potential is $V(r) = -V_0/(R_0-r)^n$ for $R_0 - r > 1$, and $V(r) = -V_0$ for $R_0 - r < 1$, where $R_0$ is the system radius. As discussed earlier, the exponent $n$ depends on the nature of the interaction—the value $n = 1$ is appropriate in the context of long-ranged strain fields [2]. For completeness, we also present here the appropriate boundary conditions at $r = R_0$ in polar coordinates:

$$\tau_0\frac{\partial}{\partial t}\psi(R_0,\phi,t) = h_1 + g\psi + \gamma\left.\frac{\partial\psi}{\partial r}\right|_{r=R_0}, \tag{60}$$

$$0 = \left\{\frac{\partial}{\partial r}\left[-\psi+\psi^3-\frac{1}{2}\nabla^2\psi+V(r)\right]+\theta_r\right\}_{r=R_0}. \tag{61}$$

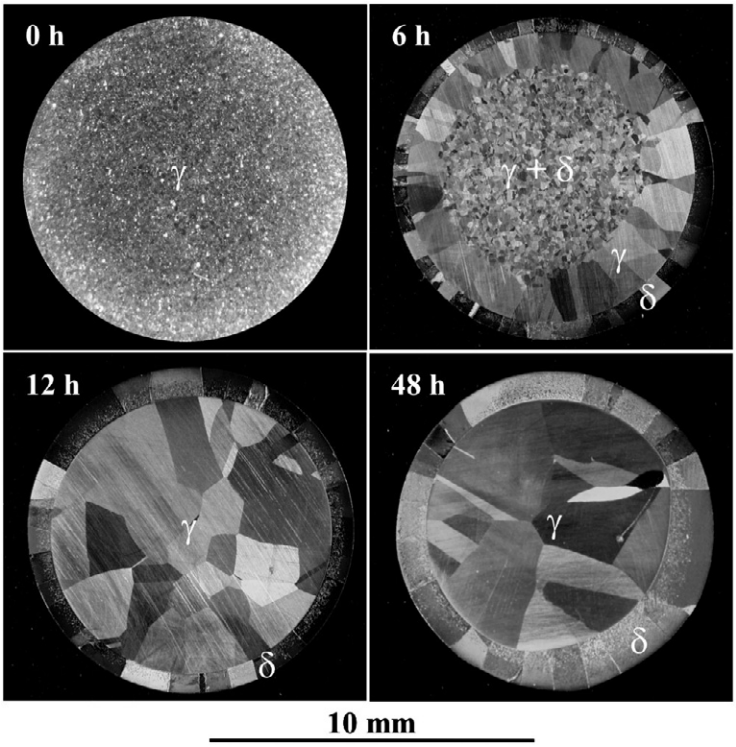


**Figure 12.** Phase separation in cylindrical samples of steel mixtures of ferrite ($\delta$, bcc) and austenite ($\gamma$, fcc) phases. The $\delta$-phase wets the open surface.

A lower cut-off on $r$ (say, $R_m$) is necessary to avoid the singularity at $r = 0$ in the Laplacian, which is

$$\nabla^2\psi = \frac{\partial^2\psi}{\partial r^2} + \frac{1}{r}\frac{\partial\psi}{\partial r} + \frac{1}{r^2}\frac{\partial^2\psi}{\partial\phi^2}. \tag{62}$$

Figure 13 shows evolution pictures obtained from a simulation of equations (59)–(61), and these are analogous to the experimental snapshots shown in figure 12. (The details of the simulation can be found in [91].) The initial condition consisted of small fluctuations about an average value of $\psi_0 = -0.2$. The phase with $\psi > 0$ wets the surface, so the wetting component is the minority phase as in section 4.2.2. This is in accordance with the phase diagram of the experimental system [91].

The evolution in figures 12 and 13 can be quantified by studying the growth dynamics of the wetting layer. Figure 14 shows the time-dependence of the wetting-layer thickness in the experiments (denoted as filled circles) and simulations (denoted as a solid curve). The growth of the ferritic wetting layer exhibits the same features as the numerical result, starting with rapid initial growth and finally reaching a plateau. There are additional experimental effects, not accounted for in the simulation, which cause quantitative deviations between the experimental and numerical results. Nevertheless, the qualitative similarity of the structural evolution is clear in figure 14. In both cases, the propagating wetting layer finally dominates over bulk domain growth.

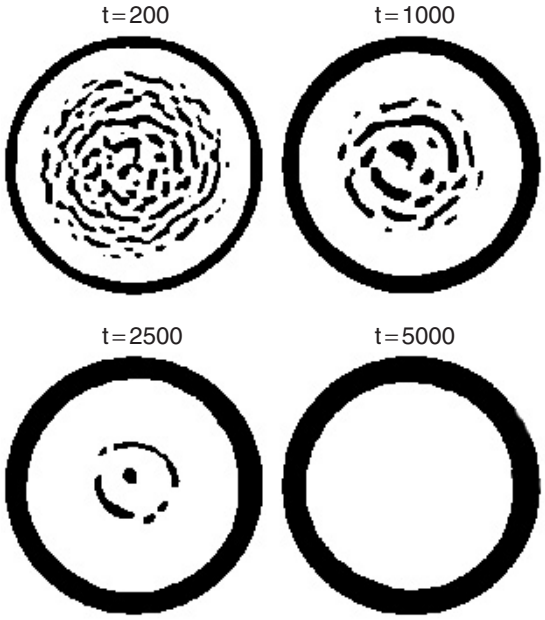


**Figure 13.** Evolution pictures obtained from a Langevin simulation of equations (59)–(61) [91]. Lattice sites with $\psi > 0$ are marked in black.

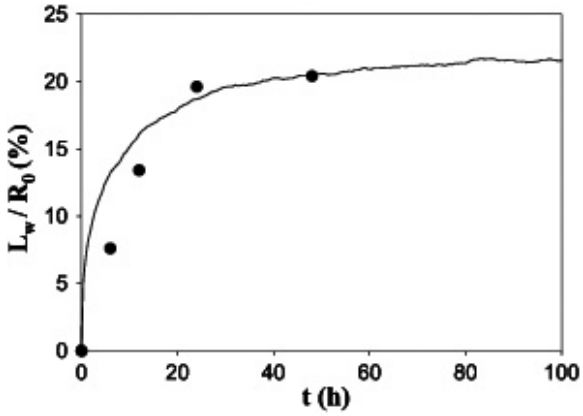


**Figure 14.** Ratio of the thickness of the wetting layer to the system radius, $R_1/R_0$, as a function of time $t$ (h). The filled circles show experimental values for the steel samples, and the solid curve was obtained from the simulation depicted in figure 13. The dimensionless simulation time was multiplied by a diffusion time $t_0 = 26.4$ s to fit the experimental data.

### *5.2. Phase separation in a thin film*

In recent work, Das *et al* [92] have undertaken Langevin and MD studies of phase separation of AB mixtures in thin films. Experimental interest in this problem has focused on two cases. One can consider a physical situation where the walls are *symmetric* and attract the same component of the mixture. Alternatively, one can consider the *antisymmetric* case, where the walls attract different components. Das *et al* have studied SDSD in both symmetric and antisymmetric films.

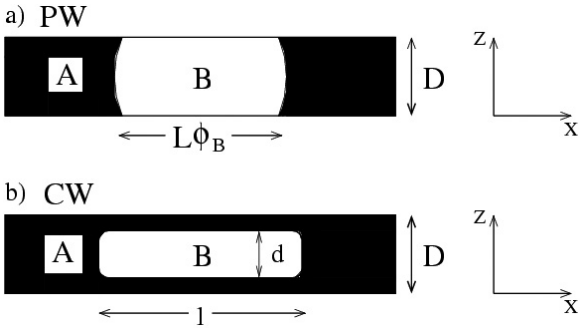


**Figure 15.** Schematic diagram of plug or partially wet (PW) and capsule/tube or completely wet (CW) states in a symmetric thin film of size $L^2 \times D$. The pictures show cross-sections of a state which is homogeneous in the $y$-direction. (a) In the PW state, both A and B are in contact with the surface. The fractions of A and B are $\phi_A$ and $\phi_B$, respectively. (b) In the CW state, B is expelled from the surface and forms a capsule of width $d$ and length $l$.

As stated earlier, the equilibrium state is either CW or PW—depending on the surface potentials and the confinement geometry [11]. For an arbitrary potential $V(z)$ (arising from the surfaces), the PW $\rightarrow$ CW crossover can be estimated as follows. Consider a thin film of lateral dimension $L^2$ with parallel surfaces at $z = 0$, $D$; and a symmetric potential such that

$$V(z) = V(D - z). \tag{63}$$

The equilibrium morphology can be either a *plug* (PW) or *capsule/tube* (CW), as depicted in figure 15. The energy associated with the PW configuration is

$$E_{\rm PW} = \int {\rm d}\vec{r}\, V(z)\psi_{\rm PW}(\vec{r}) + 2DL\sigma, \tag{64}$$

where $\psi_{\rm PW}(\vec{r})$ denotes the order parameter field, and we have neglected corrections due to the contact angle being different from $\pi/2$. We make the approximation $\psi_{\rm PW}(\vec{r}) \simeq +1$ and $-1$ in the A-rich and B-rich regions, respectively. Then

$$e_{\rm PW} = \frac{E_{\rm PW}}{L^2} \simeq (\phi_{\rm A} - \phi_{\rm B}) \int_0^D {\rm d}z\, V(z) + \frac{2D}{L}\sigma, \tag{65}$$

where $\phi_{\rm A}$ and $\phi_{\rm B}$ $(=1 - \phi_{\rm A})$ denote the fractions of A-rich and B-rich regions, respectively. We consider power-law potentials of the form

$$V(z) = -V_0 \left[ \frac{1}{(z+1)^n} + \frac{1}{(D+1-z)^n} \right], \tag{66}$$

where the potential is taken to originate behind the surfaces. Then (for $n > 1$)

$$e_{\rm PW} = (\phi_{\rm A} - \phi_{\rm B}) \frac{2V_0}{n-1} [(D+1)^{-n+1} - 1] + \frac{2D}{L}\sigma. \tag{67}$$

On the other hand, for the CW morphology shown in figure 15, the capsule thickness $d$ $(<D)$ is an additional parameter. The corresponding energy is obtained as

$$E_{\rm CW} = \int {\rm d}\vec{r}\, V(z)\psi_{\rm CW}(\vec{r}) + 2(l+d)L\sigma, \tag{68}$$

where $l$ is the length of the B-capsule. This is determined by the composition constraint as

$$l = \frac{\phi_{\rm B} L D}{d}, \tag{69}$$

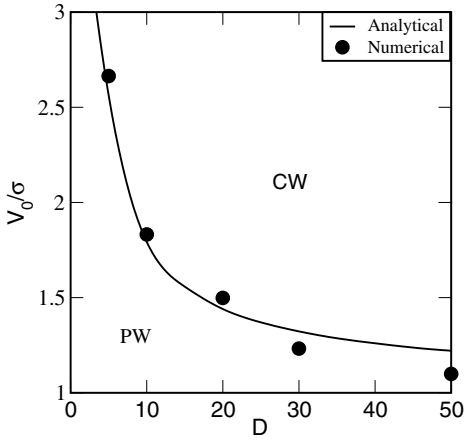


**Figure 16.** Phase diagram in the $(D, V_0/\sigma)$-plane for a binary mixture in a symmetric thin film. The states are labelled as partially wet (PW) and completely wet (CW), and are shown in figure 15. The solid curve denotes the PW $\rightarrow$ CW crossover obtained from equation (72) for a power-law potential with $n = 3$. The filled circles denote the PW $\rightarrow$ CW boundary obtained from Langevin simulations with a plug initial condition, as described in the text.

and must satisfy $l \leqslant L$. Thus

$$e_{\rm CW} = \frac{E_{\rm CW}}{L^2} \simeq \frac{(L-l)}{L}\int_0^D {\rm d}z\, V(z) + \frac{l}{L}\left[\int_0^{\frac{D-d}{2}} {\rm d}z\, V(z) - \int_{\frac{D-d}{2}}^{\frac{D+d}{2}} {\rm d}z\, V(z) + \int_{\frac{D+d}{2}}^{D} {\rm d}z\, V(z)\right] + \frac{2(l+d)\sigma}{L}. \tag{70}$$

For the power-law potential in equation (66)

$$e_{\rm CW} = \frac{2V_0}{n-1}\left\{(D+1)^{-n+1} - 1 + \frac{2\phi_{\rm B}D}{d}\left[\left(\frac{D-d}{2}+1\right)^{-n+1} - \left(\frac{D+d}{2}+1\right)^{-n+1}\right]\right\} + 2\left(\frac{\phi_{\rm B}D}{d} + \frac{d}{L}\right)\sigma. \tag{71}$$

In the $L \rightarrow \infty$ limit, we neglect terms of $\mathrm{O}(D/L)$ in equation (67) and $\mathrm{O}(d/L)$ in equation (71). The optimal value of $d$ (denoted as $d_m$) is obtained by minimizing $e_{\rm CW}$ subject to the constraint $\phi_{\rm B}D \leqslant d_m < 1$. The crossover from the PW $\rightarrow$ CW morphology occurs when

$$e_{\rm PW} = e_{\rm CW}(d_m), \tag{72}$$

where we have neglected fluctuations at low temperatures. The resultant phase diagram for $n = 3$ in $(D, V_0/\sigma)$-space is shown in figure 16. The solid circles in figure 16 denote results from Langevin simulations on systems of size $512^2 \times D$ [92]. These were done by setting up a plug initial condition, which was allowed to evolve for different values of the surface field. The circles in figure 16 denote the smallest field value where the plug asymptotically evolves into a capsule state. We make two observations in connection with this phase diagram.

(1) For $D \rightarrow \infty$, the condition in equation (72) reduces to Young's condition in the bulk for the case of a power-law potential:

$$\frac{2V_0}{n-1} = \sigma. \tag{73}$$

For $n = 3$, the appropriate limiting value is $V_0/\sigma = 1$, as seen in figure 16.

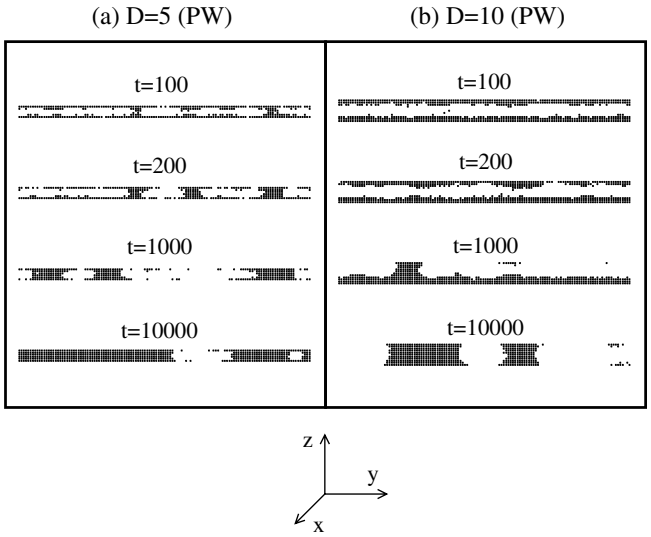


**Figure 17.** Phase separation of a critical mixture in a symmetric thin film of size $L^2 \times D$ with $L = 512$ and $D = 5, 10$. The evolution snapshots are obtained from an Euler-discretized version of equation (28) with $\Delta x = 1$, $\Delta t = 0.02$. The boundary conditions in equation (31) with $\tau_0 = 0$ and equation (32) are implemented at $z = 0$, $D$, and periodic boundary conditions are imposed in the other directions. The potential $V(z)$ is of the form in equation (66) with $V_0 = 0.1$ and $n = 3$, and gives a PW morphology for $D = 5, 10$. The other parameter values are the same as in figure 4.

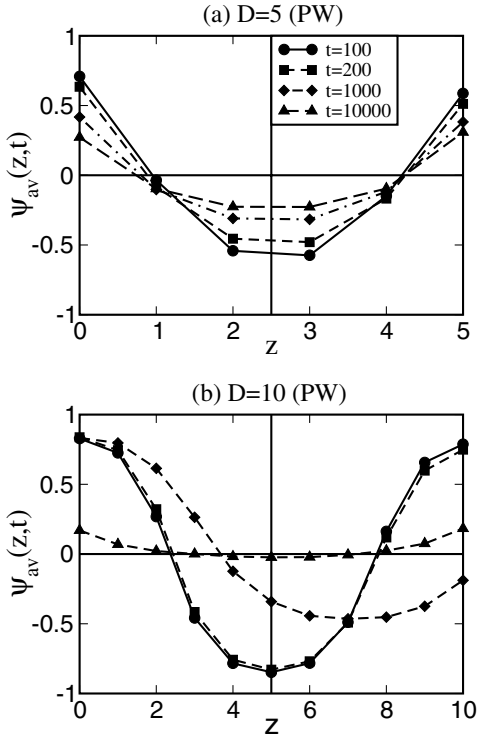


**Figure 18.** Laterally averaged profiles for the evolution depicted in figure 17 at dimensionless times $t = 100, 200, 1000, 10\,000$.

(2) The numerical results in figure 16 underestimate the PW → CW crossover at larger values of $D$, because the $O(D/L)$ terms become appreciable. Recall that we have neglected these in the above discussion.

Das *et al* have obtained a good understanding of the segregation kinetics in both the diffusive and hydrodynamic cases. Here, we only show representative results from their studies. Figure 17 shows evolution pictures for diffusive phase separation in a symmetric film. The parameters are chosen so that the surfaces are PW in equilibrium. The frames on the LHS and RHS show symmetric films with $D = 5$ and 10, respectively. Notice that the rapid kinetics of surface enrichment (see section 6) results in a metastable CW state. This state can be very long lived, depending on the proximity to the PW–CW line in the phase diagram. The CW state is finally broken up by fluctuations, and coarsening proceeds by the lateral diffusion of symmetric plugs. The crossover time to the PW state is earlier for smaller values of $D$. In figure 18, we show the corresponding evolution of the laterally averaged profiles.

In figures 19 and 20, we show analogous results for the CW morphology, where segregation proceeds by the coarsening of capsules. Das *et al* have obtained detailed results for the layer-wise correlation functions and length scales which characterize the evolution shown in figures 17 and 19. They have also obtained results for antisymmetric films, and the case with hydrodynamics. These results will be presented in a forthcoming publication [92].

## 6. Kinetics of surface enrichment for stable binary mixtures

### *6.1. General solution of linear problem*

Let us now consider the problem of surface enrichment, which has already been referred to earlier. This occurs when a stable binary mixture (with $T > T_c$) is placed in contact with a surface (at $z = 0$) which prefers one of the components. For large $z$, the stable mixture continues to be homogeneous. However, the surface becomes enriched in the preferred component, resulting in a time-dependent profile which propagates into the bulk. Jones *et al* [57, 58] have studied the kinetics of surface enrichment for polymer mixtures, and found that the enrichment profiles are characterized by diffusive length-scales. There have also been numerical studies of this problem with both short-ranged and long-ranged surface fields via MC [43] and Langevin [93] simulations. Furthermore, Binder and Frisch [48] have studied this problem for a short-ranged surface potential in the framework of a linear theory. Following Frisch *et al* [94, 95], we discuss the solution of the linear problem for a large class of surface potentials. The regime of validity and the properties of this solution are also discussed.

Recall the nonlinear model in equations (28)–(32). Consider its deterministic version with $T = 0$. We will study the evolution of an initial condition consisting of fluctuations about a uniform background, namely, $\psi = \psi_0 + \psi'$, as discussed in section 4.1. If we linearize equation (28) in the fluctuation field $\psi'$, we obtain (dropping the primes)

$$\frac{\partial}{\partial t}\psi(\vec{r},t) = -\nabla^2\left[C\psi + \frac{1}{2}\nabla^2\psi - V(z)\right], \qquad z > 0, \tag{74}$$

where we have introduced the parameter

$$C = \mathrm{sgn}(T_c - T) - 3\psi_0^2. \tag{75}$$

The linearized boundary conditions are as follows:

$$\tau_0\frac{\partial}{\partial t}\psi(\vec{\rho},0,t) = h_1 + g\psi_0 + g\psi + \gamma\left.\frac{\partial\psi}{\partial z}\right|_{z=0}, \tag{76}$$

$$0 = \frac{\partial}{\partial z}\left[C\psi + \frac{1}{2}\nabla^2\psi - V(z)\right]\Bigg|_{z=0}. \tag{77}$$

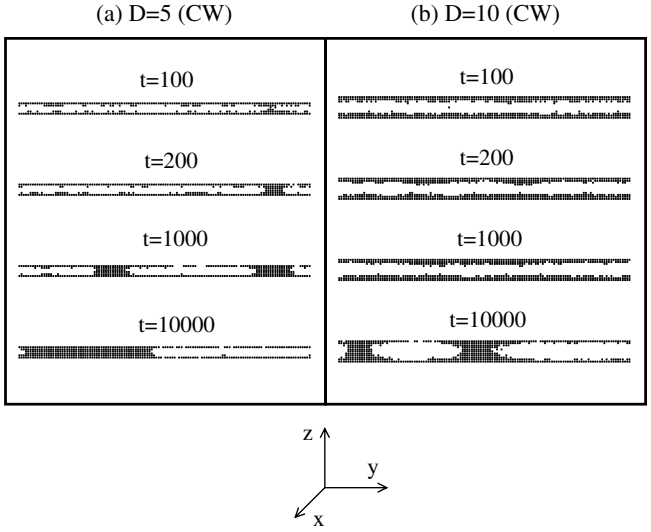


**Figure 19.** Analogous to figure 17, but for the completely wet case with $V_0 = 0.4$ and $n = 3$.

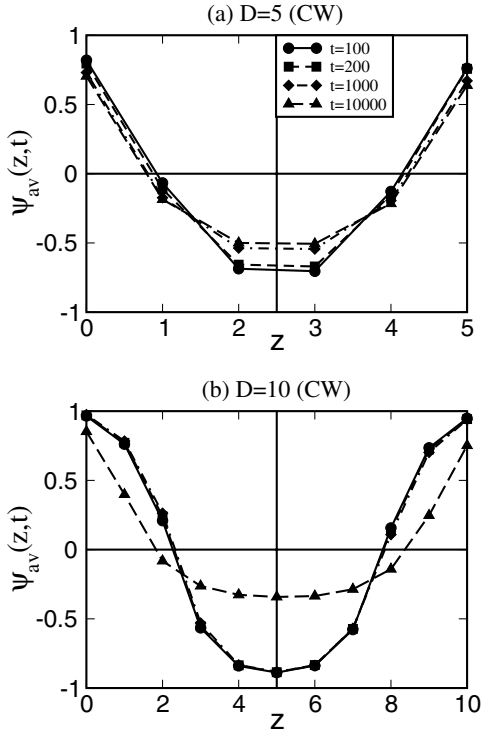


**Figure 20.** Analogous to figure 18, but for the evolution shown in figure 19.

Here, we have explicitly incorporated the possibility that $T$ may be above or below $T_c$ by using the sign-function, $\mathrm{sgn}(x) = x/|x|$. In our discussion of SDSD, we used the static version ($\tau_0 = 0$) of equation (31). Here, we retain the dynamical version, as we are interested in the

time-dependent behaviour of the order parameter at the surface. Finally, we focus on potentials which are flat at the origin, so $V'(0)$ is subsequently set to zero in equation (77).

For $T < T_c$, the fluctuations grow in time (when $3\psi_0^2 < 1$) and the linearized equations are not valid after the early-time regime. For $T > T_c$, the fluctuations do not grow and equations (74)–(77) are valid for all time—provided that the surface field is sufficiently weak that the value of $\psi$ stays small even near the surface. Thus, our analysis of the linearized model will be valid at early times for arbitrary temperatures; and at late times when $T > T_c$ and the surface field is weak. Furthermore, the solution of the linearized model is also valid for $T < T_c$ and highly off-critical quenches ($3\psi_0^2 - 1 \gg 0$) provided that there is no nucleation of droplets. This case was discussed in sections 4.2.2 and 4.2.3.

A Fourier transform of equations (74)–(77) in the direction parallel to the wall yields the following equations:

$$\frac{\partial}{\partial t}\psi(\vec{k}_\parallel, z, t) = \left(C - \frac{1}{2}\vec{k}_\parallel^2\right)\vec{k}_\parallel^2\psi - \left(C - \vec{k}_\parallel^2\right)\frac{\partial^2\psi}{\partial z^2} - \frac{1}{2}\frac{\partial^4\psi}{\partial z^4} + V''(z)\delta(\vec{k}_\parallel), \tag{78}$$

$$\tau_0\frac{\partial}{\partial t}\psi(\vec{k}_\parallel, 0, t) = (h_1 + g\psi_0)\delta(\vec{k}_\parallel) + g\psi + \gamma\left.\frac{\partial\psi}{\partial z}\right|_{z=0}, \tag{79}$$

$$0 = \frac{\partial}{\partial z}\left[\left(C - \frac{1}{2}\vec{k}_\parallel^2\right)\psi + \frac{1}{2}\frac{\partial^2\psi}{\partial z^2}\right]\Bigg|_{z=0}, \tag{80}$$

where $\vec{k}_\parallel$ denotes the wavevector parallel to the surface. If we include a surface diffusion term, the parameter $g$ in the second term on the RHS of equation (79) is modified [60].

To be specific, we consider critical binary mixtures (namely, $\psi_0 = 0$) and focus on the case with $T > T_c$. The solution trivially generalizes to cases with arbitrary $\psi_0$ and $T < T_c$. Furthermore, we consider the case where the order-parameter field is homogeneous parallel to the surface (namely, $\psi(\vec{\rho}, z, t) \equiv \psi(z, t)$). This is reasonable because the bulk is homogeneous, and the surface field promotes homogeneity at the surface. In any case, the method of solution outlined below is also applicable to the laterally inhomogeneous case, with an appropriate modification of parameters. This is apparent from a comparison of equations (78)–(80) with the laterally homogeneous version.

Thus, the relevant model is equations (78)–(80) with $\psi_0 = 0$, $T > T_c$, and $\vec{k}_\parallel = 0$:

$$\frac{\partial}{\partial t}\psi(z, t) = \frac{\partial^2\psi}{\partial z^2} - \frac{1}{2}\frac{\partial^4\psi}{\partial z^4} + V''(z), \qquad z > 0, \tag{81}$$

$$\tau_0\frac{\partial}{\partial t}\psi(0, t) = h_1 + g\psi + \gamma\left.\frac{\partial\psi}{\partial z}\right|_{z=0}, \tag{82}$$

$$0 = \left.\frac{\partial\psi}{\partial z}\right|_{z=0} - \frac{1}{2}\left.\frac{\partial^3\psi}{\partial z^3}\right|_{z=0}. \tag{83}$$

We Laplace-transform equations (81)–(83) in time to obtain

$$s\tilde{\psi}(z, s) = \frac{\partial^2\tilde{\psi}}{\partial z^2} - \frac{1}{2}\frac{\partial^4\tilde{\psi}}{\partial z^4} + \frac{V''(z)}{s}, \qquad z > 0, \tag{84}$$

$$s\tilde{\psi}(0, s) = \frac{h_1}{s} + g\tilde{\psi} + \gamma\left.\frac{\partial\tilde{\psi}}{\partial z}\right|_{z=0}, \tag{85}$$

$$0 = \left.\frac{\partial\tilde{\psi}}{\partial z}\right|_{z=0} - \frac{1}{2}\left.\frac{\partial^3\tilde{\psi}}{\partial z^3}\right|_{z=0}, \tag{86}$$

where

$$\tilde{\psi}(z, s) = \int_0^\infty \mathrm{d}t\, \mathrm{e}^{-st}\psi(z, t), \tag{87}$$

and we have used the homogeneous initial condition $\psi(z, t = 0) = 0$. The timescale $\tau_0$ has been absorbed into the definition of the parameters $h_1, g, \gamma$.

Equation (84) is an inhomogeneous fourth-order differential equation with two boundary conditions. The solution of equations (84)–(86) can be obtained using the solutions of the homogeneous part of equation (84) [96]. The final result is as follows [94]:

$$\begin{aligned}\tilde{\psi}(z,s) = {} & \frac{h_1\xi_- + 2s(s-g)(\xi_+\alpha - \xi_-\beta)\xi_-}{D(s)} e^{-z/\xi_+} - \xi_+\alpha e^{-z/\xi_+} \\ & - \frac{h_1\xi_+ + 2s(s-g)(\xi_+\alpha - \xi_-\beta)\xi_+}{D(s)} e^{-z/\xi_-} + \xi_-\beta e^{-z/\xi_-} \\ & - \frac{\xi_+}{s\Delta}\left[e^{-z/\xi_+}\int_0^z dz'\, e^{z'/\xi_+}V''(z') + e^{z/\xi_+}\int_z^\infty dz' e^{-z'/\xi_+}V''(z')\right] \\ & + \frac{\xi_-}{s\Delta}\left[e^{-z/\xi_-}\int_0^z dz'\, e^{z'/\xi_-}V''(z') + e^{z/\xi_-}\int_z^\infty dz'\, e^{-z'/\xi_-}V''(z')\right], \end{aligned} \tag{88}$$

where

$$\begin{aligned} \alpha &= \frac{1}{s\Delta}\int_0^\infty dz'\, e^{-z'/\xi_+}V''(z'), \\ \beta &= \frac{1}{s\Delta}\int_0^\infty dz'\, e^{-z'/\xi_-}V''(z'), \\ \Delta &= \xi_+^{-2} - \xi_-^{-2}, \qquad \xi_\pm^{-2} = 1 \pm \sqrt{1-2s}, \\ D(s) &= \frac{\sqrt{s}(s-g)}{\sqrt{2}}(\xi_+^{-1} - \xi_-^{-1}) + \gamma\sqrt{2s}\sqrt{1-2s}. \end{aligned} \tag{89}$$

The first four terms on the RHS of equation (88) arise from the homogeneous part of equation (84), with $\xi_+$ and $\xi_-$ being $s$-dependent length scales. The terms involving integrals over $V''(z)$ in equation (88) arise from the particular solution of equation (84).

The expression in equation (88) is unwieldy and has to be inverse-transformed numerically to obtain the temporal evolution of enrichment profiles. However, it is relatively straightforward to obtain the asymptotic time-dependence of important profile characteristics. Recall that we are primarily interested in potentials which exhibit power-law decays, i.e., $V(z) \sim -z^{-n}$.

### *6.2. Properties of enrichment profiles*

An important profile characteristic is the time-dependence of $\psi(0, t)$, the value of the order parameter at the surface. To obtain this, we set $z = 0$ in equation (88) and obtain

$$\tilde{\psi}(0,s) = \frac{h_1(\xi_- - \xi_+) - 2(\xi_+\alpha - \xi_-\beta)\gamma\sqrt{2s}\sqrt{1-2s}}{s(s-g)(\xi_- - \xi_+) + \gamma\sqrt{2s}\sqrt{1-2s}}. \tag{90}$$

The asymptotic ($t \to \infty$) behaviour of $\psi(0, t)$ is determined by the $s \to 0$ behaviour of $\tilde{\psi}(0, s)$. To ascertain this, the leading $s$-dependence (as $s \to 0$) of various quantities on the

RHS of equation (90) is computed as follows:

$$\begin{aligned}
\xi_- &= \frac{1}{\sqrt{s}}[1+\mathrm{O}(s)],\\
\xi_+ &= \frac{1}{\sqrt{2}}[1+\mathrm{O}(s)],\\
\alpha &= -\frac{A}{2s}+\mathrm{O}(1), \qquad A = -\int_0^\infty \mathrm{d}z\, \mathrm{e}^{-z\sqrt{2}} V''(z),\\
\beta &= \frac{h_1}{2\sqrt{s}} - \frac{B}{2} + \mathrm{O}(\sqrt{s}), \qquad B = -\int_0^\infty \mathrm{d}z\, V(z).
\end{aligned} \tag{91}$$

Replacing these in equation (90), we obtain

$$\begin{aligned}
\tilde{\psi}(0,s) = \frac{1}{s}&\left(\frac{h_1 + A\gamma + h_1\gamma\sqrt{2}}{\gamma\sqrt{2}-g}\right)\\
&- \frac{1}{\sqrt{s}}\frac{1}{(\gamma\sqrt{2}-g)}\left[\frac{g(h_1+A\gamma+h_1\gamma\sqrt{2})}{\sqrt{2}(\gamma\sqrt{2}-g)} - \frac{h_1}{\sqrt{2}} - B\gamma\sqrt{2}\right] + \mathrm{O}(1).
\end{aligned} \tag{92}$$

The asymptotic time-dependence of $\psi(0,t)$ is obtained by inverse-transforming $\tilde{\psi}(0,s)$ as follows:

$$\begin{aligned}
\psi(0,t) = &\left(\frac{h_1 + A\gamma + h_1\gamma\sqrt{2}}{\gamma\sqrt{2}-g}\right)\\
&- \frac{1}{\sqrt{\pi}(\gamma\sqrt{2}-g)}\left[\frac{g(h_1+A\gamma+h_1\gamma\sqrt{2})}{\sqrt{2}(\gamma\sqrt{2}-g)} - \frac{h_1}{\sqrt{2}} - B\gamma\sqrt{2}\right] t^{-1/2},
\end{aligned} \tag{93}$$

where we have retained only the leading correction to the constant value of $\psi(0,t)$ as $t\to\infty$. Thus, $\psi(0,t)$ saturates diffusively to its equilibrium value.

Next, consider the $s$-dependence of the profile moments:

$$\langle z^m\rangle = \int_0^\infty \mathrm{d}z\, z^m \tilde{\psi}(z,s). \tag{94}$$

Replacing the functional form for $\tilde{\psi}(z,s)$ from equation (88) in equation (94), some algebra leads to the following result:

$$\begin{aligned}
\langle z^m\rangle = &\Gamma(m+1)\xi_+^{m+1}\left[\frac{h_1\xi_- + 2s(s-g)(\xi_+\alpha-\xi_-\beta)\xi_-}{D(s)} - \xi_+\alpha\right]\\
&- \Gamma(m+1)\xi_-^{m+1}\left[\frac{h_1\xi_+ + 2s(s-g)(\xi_+\alpha-\xi_-\beta)\xi_+}{D(s)} - \xi_-\beta\right]\\
&- \frac{\xi_+}{s\Delta}\int_0^\infty \mathrm{d}z\, V''(z)\left[\int_0^\infty \mathrm{d}x\, \mathrm{e}^{-x/\xi_+}(z+x)^m + \int_0^z \mathrm{d}x\, \mathrm{e}^{-x/\xi_+}(z-x)^m\right]\\
&+ \frac{\xi_-}{s\Delta}\int_0^\infty \mathrm{d}z\, V''(z)\left[\int_0^\infty \mathrm{d}x\, \mathrm{e}^{-x/\xi_-}(z+x)^m + \int_0^z \mathrm{d}x\, \mathrm{e}^{-x/\xi_-}(z-x)^m\right].
\end{aligned} \tag{95}$$

Clearly, moments are not defined to all orders for power-law potentials. Thus, for a potential $V(z)\sim -z^{-n}$, moments are only defined upto $\langle z^n\rangle$. The asymptotic behaviour of $\langle z^m\rangle$ as $t\to\infty$ is determined by the leading terms in equation (95) as $s\to 0$. The dominant contributions arise from the second, fifth and sixth terms on the RHS of equation (95), and are

$O[s^{-(m+3)/2}]$ and $O[s^{-(m+2)/2}]$. However, there is a cancellation of $O[s^{-(m+3)/2}]$ contributions. The final result, to leading order, is

$$\langle z^m \rangle = \frac{1}{s^{\frac{m}{2}+1}} \Gamma(m+1) \left[ \frac{h_1\sqrt{2} + g(A + h_1\sqrt{2})}{2(\gamma\sqrt{2} - g)} + B \right]. \tag{96}$$

Finally, the expression in equation (96) is inverse-transformed to obtain the leading asymptotic time-dependence as

$$\langle z^m \rangle = -\frac{\Gamma(m+1)}{\Gamma(\frac{m}{2}+1)} \left[ \frac{h_1\sqrt{2} + g(A + h_1\sqrt{2})}{2(\gamma\sqrt{2} - g)} + B \right] t^{m/2}, \tag{97}$$

which also corresponds to diffusive behaviour.

The results presented here show a universal time-dependence of $\psi(0, t)$ and $\langle z^m \rangle$ for a wide range of potentials. Of course, these results have been obtained in the context of a linear theory. There is a range of *weak* surface fields where there is no appreciable difference between the analytical results obtained from the linear model and numerical results from the full nonlinear model [94, 95]. In this regime, equation (88) constitutes a complete solution of the surface enrichment problem. As the field strength is increased, the validity of linear theory breaks down in the vicinity of the surface. Though this is true for the time-dependent profiles, Frisch *et al* [94] demonstrated that the diffusive behaviour of various profile characteristics is unaffected, even in the strongly nonlinear regime.

## 7. Summary and discussion

Let us conclude this review with a summary and discussion of the results presented here. We have focused on the problem of *surface-directed spinodal decomposition* (SDSD), namely, the interplay of wetting and phase separation for an unstable binary (AB) mixture in contact with a surface which has a preferential attraction for one of the components (say, A). The surface is either *partially wetted* or *completely wetted* by the preferred component, depending on the relative strengths of the A–B, A–surface and B–surface surface tensions. The system evolves from its unstable homogeneous state to the equilibrium morphology by the formation of SDSD waves, which propagate from the surface into the bulk. The evolution of these SDSD waves is driven by phase separation in the bulk. In turn, domain growth adjacent to the surface is affected by the layered morphology at the surface.

The SDSD problem is of great experimental and technological importance. Therefore, we started this paper by providing an overview of important experiments in this area. This overview clarifies the issues which must be addressed by theoretical studies of this problem. Subsequently, we reviewed the theoretical modelling of SDSD. For diffusive phase separation, we can study either microscopic models, e.g., the spin-exchange kinetic Ising model in contact with a surface; or coarse-grained models, e.g., the Cahn–Hilliard–Cook equation supplemented by boundary conditions which model the presence of a surface. These models can be easily extended to study SDSD in binary fluids, where the hydrodynamic velocity field determines the intermediate and asymptotic behaviours of the phase-separating system.

We have used these models to discuss the wetting-layer kinetics, and domain-growth kinetics adjacent to the wetting layer. We have also presented numerical results for SDSD in a semi-infinite geometry for a wide range of mixture compositions. The growth law for the wetting layer exhibits a crossover from potential-dependent growth at early times to a universal growth regime at late times. The asymptotic growth is fastest for the case where there is only a small fraction of the wetting component. On the other hand, the wetting-layer

growth is slowest when the wetting component is the majority component, because droplets of the minority phase compete with the wetting layer.

Our modelling extends naturally to the problem of phase separation in a confined geometry (e.g., thin film), where novel physical effects arise due to the interplay of SDSD waves arising from different boundaries. In this review, we have also presented results for SDSD in a cylindrical geometry and a thin-film geometry.

Finally, we turned our attention to the problem of *surface-enrichment kinetics*. This occurs when a stable binary mixture (with $T > T_c$) is placed in contact with a surface which prefers one of the components. As before, the surface is enriched by the preferred component though the bulk remains homogeneous in this case. The kinetics of surface enrichment is also of considerable experimental interest. For weak surface fields, a linearization approximation is valid, and we present the corresponding solution of the enrichment problem for a wide class of surface potentials. The general solution is characterized by the following features. The surface value of the enrichment profile saturates diffusively to its asymptotic value. Furthermore, the profile moments also grow diffusively in time. The substantive features of this solution remain valid even for strong surface fields, though the linearization approximation is no longer valid near the surface.

As this review demonstrates, we have now gained a good understanding of the interplay of wetting and phase separation at surfaces. However, there remain many open questions, which offer both theoretical and experimental challenges. In particular, we need a better understanding of phase-separation kinetics in confined systems. Further, the geometries considered here have been relatively simple, but more complex geometries, e.g., wedges, patterned surfaces, etc, are often encountered in experimental situations. To date, we only have a preliminary understanding of segregation dynamics in these complicated geometries. It is our hope that this review will motivate further interest in this fascinating field of research.

## Acknowledgments

The author is grateful to Kurt Binder and Harry Frisch for a very productive collaboration on the problems discussed in this review. He is also grateful to his other coworkers for fruitful collaborations on these problems, in particular B Aichmayer, S Bastea, S K Das, P Fratzl, J Horbach, J L Lebowitz, P Nielaba and G Saller. He thanks S K Das for assistance in preparing the figures for SDSD in thin films.

## References

[1] Bray A J 1994 *Adv. Phys.* **43** 357
[2] Binder K and Fratzl P 2001 *Phase Transformations in Materials* ed G Kostorz (Weinheim: Wiley–VCH) p 409
[3] Dattagupta S and Puri S 2004 *Dissipative Phenomena in Condensed Matter: Some Applications* (Heidelberg: Springer)
[4] Young T 1805 *Phil. Trans. R. Soc.* A **95** 69
[5] Cahn J W 1977 *J. Chem. Phys.* **66** 3667
[6] Nakanishi H and Fisher M E 1982 *Phys. Rev. Lett.* **49** 1565
[7] Binder K 1983 *Phase Transitions and Critical Phenomena* vol 8, ed C Domb and J L Lebowitz (London: Academic) p 1
[8] de Gennes P G 1985 *Rev. Mod. Phys.* **57** 827
[9] Diehl H W 1986 *Phase Transitions and Critical Phenomena* vol 10, ed C Domb and J L Lebowitz (London: Academic) p 75
[10] Dietrich S 1988 *Phase Transitions and Critical Phenomena* vol 12, ed C Domb and J L Lebowitz (London: Academic) p 1
[11] Liu A J, Durian D J, Herbolzheimer E and Safran S A 1990 *Phys. Rev. Lett.* **65** 1897
Monette L, Liu A J and Grest G S 1992 *Phys. Rev.* A **46** 7664

[12] Puri S and Frisch H L 1997 *J. Phys.: Condens. Matter* **9** 2109
[13] Binder K 1998 *J. Non-Equilib. Thermodyn.* **23** 1
[14] Krausch G 1995 *Mater. Sci. Eng. Rep.* **R14** 1
[15] Geoghegan M and Krausch G 2003 *Prog. Polym. Sci.* **28** 261
[16] Jones R A L, Norton L J, Kramer E J, Bates F S and Wiltzius P 1991 *Phys. Rev. Lett.* **66** 1326
[17] Krausch G, Dai C-A, Kramer E J and Bates F S 1993 *Phys. Rev. Lett.* **71** 3669
[18] Bruder F and Brenn R 1992 *Phys. Rev. Lett.* **69** 624
[19] Straub W, Bruder F, Brenn R, Krausch G, Bielefeldt H, Kirsch A, Marti O, Mlynek J L and Marko J F 1995 *Europhys. Lett.* **29** 353
[20] Krausch G, Mlynek J, Straub W, Brenn R and Marko J F 1994 *Europhys. Lett.* **28** 323
[21] Geoghegan M, Jones R A L and Clough A S 1995 *J. Chem. Phys.* **103** 2719
[22] Geoghegan M, Ermer H, Jüngst G, Krausch G and Brenn R 2000 *Phys. Rev.* E **62** 940
[23] Karim A, Douglas J F, Lee B P, Glotzer S C, Rogers J A, Jackman R J, Amis E J and Whitesides G M 1998 *Phys. Rev.* E **57** R6273
[24] Ermi B D, Nisato G, Douglas J F, Rogers J A and Karim A 1998 *Phys. Rev. Lett.* **81** 3900
[25] Böltau M, Walheim S, Mlynek J, Krausch G and Steiner U 1998 *Nature* **391** 877
[26] Siggia E D 1979 *Phys. Rev.* A **20** 595
[27] Furukawa H 1985 *Phys. Rev.* A **31** 1103
Furukawa H 1985 *Adv. Phys.* **34** 703
[28] Wiltzius P and Cumming A 1991 *Phys. Rev. Lett.* **66** 3000
[29] Cumming A, Wiltzius P, Bates F S and Rosedale J H 1992 *Phys. Rev.* A **45** 885
[30] Shi B Q, Harrison C and Cumming A 1993 *Phys. Rev. Lett.* **70** 206
[31] Harrison C, Rippard W and Cumming A 1995 *Phys. Rev.* E **52** 723
[32] Ma W-J, Keblinski P, Maritan A, Koplik J and Banavar J R 1993 *Phys. Rev.* E **48** R2362
[33] Keblinski P, Ma W-J, Maritan A, Koplik J and Banavar J R 1994 *Phys. Rev. Lett.* **72** 3738
[34] Guenoun P, Beysens D and Robert M 1990 *Phys. Rev. Lett.* **65** 2406
Guenoun P, Beysens D and Robert M 1991 *Physica* A **172** 137
[35] Tanaka H 1993 *Phys. Rev. Lett.* **70** 53
Tanaka H 1993 *Phys. Rev. Lett.* **70** 2770
Tanaka H 1993 *Europhys. Lett.* **24** 665
[36] Tanaka H 2001 *J. Phys.: Condens. Matter* **13** 4637
[37] Bussemaker H 1995 Pattern formation and correlations in lattice gas automata *PhD Thesis* University of Utrecht
[38] Velasco E and Toxvaerd S 1993 *Phys. Rev. Lett.* **71** 388
Velasco E and Toxvaerd S 1994 *J. Phys.: Condens. Matter* **6** A205
[39] Hohenberg P C and Halperin B I 1977 *Rev. Mod. Phys.* **49** 435
[40] Binder K 1974 *Z. Phys.* **267** 313
[41] Xiong G M and Gong C D 1989 *Phys. Rev.* B **39** 9384
[42] Langer J S, Bar-on M and Miller H D 1975 *Phys. Rev.* A **11** 1417
[43] Jiang Z and Ebner C 1989 *Phys. Rev.* B **39** 2501
[44] Ball R C and Essery R L H 1990 *J. Phys.: Condens. Matter* **2** 10303
[45] Weeks J D 1980 *Ordering in Strongly Fluctuating Condensed Matter Systems* ed T Riste (New York: Plenum) p 293
[46] Van Beijeren H and Nolden I 1987 *Structure and Dynamics of Surfaces* vol 2, ed W Schommers and P Blanckenhagen (Heidelberg: Springer) p 259
[47] Binder K and Hohenberg P C 1972 *Phys. Rev.* B **6** 3461
[48] Binder K and Frisch H L 1991 *Z. Phys.* B **84** 403
[49] Puri S and Binder K 1992 *Phys. Rev.* A **46** R4487
Puri S and Binder K 1994 *Phys. Rev.* E **49** 5359
[50] Schmidt I and Binder K 1987 *Z. Phys.* B **67** 369
[51] Puri S and Binder K 1992 *Z. Phys.* B **86** 263
[52] Puri S and Binder K 1994 *J. Stat. Phys.* **77** 145
[53] Bhattacharya A, Rao M and Chakrabarti A 1994 *Phys. Rev.* E **49** 524
[54] Vaksman M A and McMullen W E 1994 *Phys. Rev.* E **49** 4724
[55] Diehl H W and Janssen H K 1992 *Phys. Rev.* A **45** 7145
[56] Oono Y and Puri S 1987 *Phys. Rev. Lett.* **58** 836
Oono Y and Puri S 1988 *Phys. Rev.* A **38** 434
Puri S and Oono Y 1988 *Phys. Rev.* A **38** 1542
Puri S and Oono Y 1988 *J. Phys. A: Math. Gen.* **21** L755

[57] Jones R A L, Kramer E J, Rafailovich M H, Sokolov J and Schwarz S A 1989 *Phys. Rev. Lett.* **62** 280
[58] Jones R A L and Kramer E J 1990 *Phil. Mag.* B **62** 129
[59] Frisch H L, Nielaba P and Binder K 1995 *Phys. Rev.* E **52** 2848
[60] Fischer H P, Maass P and Dieterich W 1997 *Phys. Rev. Lett.* **79** 893
[61] Puri S and Binder K 2001 *Phys. Rev. Lett.* **86** 1797
Puri S and Binder K 2002 *Phys. Rev.* E **66** 061602
[62] Puri S, Binder K and Frisch H L 1997 *Phys. Rev.* E **56** 6991
[63] Dzyaloshinskii I E, Lifshitz E M and Pitaevskii L P 1961 *Adv. Phys.* **10** 165
[64] Lipowsky R 1985 *J. Phys. A: Math. Gen.* **18** L585
[65] Puri S 1988 *Phys. Lett.* A **134** 205
[66] Lipowsky R and Huse D A 1986 *Phys. Rev. Lett.* **57** 353
[67] Brown G and Chakrabarti A 1992 *Phys. Rev.* A **46** 4829
[68] Brown G, Chakrabarti A and Marko J F 1994 *Phys. Rev.* E **50** 1674
[69] Brown G and Chakrabarti A 1994 *J. Chem. Phys.* **101** 3310
Brown G and Chakrabarti A 1995 *J. Chem. Phys.* **102** 1440
[70] Oono Y and Shiwa Y 1987 *Mod. Phys. Lett.* B **1** 49
[71] Oono Y and Bahiana M 1988 *Phys. Rev. Lett.* **61** 1109
[72] Marko J F 1993 *Phys. Rev.* E **48** 2861
[73] Sagui C, Somoza A M, Roland C and Desai R C 1993 *J. Phys. A: Math. Gen.* **26** L1163
[74] Lee B P, Douglas J F and Glotzer S C 1999 *Phys. Rev.* E **60** 5812
[75] Zhang Z and Chakrabarti A 1994 *Phys. Rev.* E **50** R4290
[76] Chen H and Chakrabarti A 1997 *Phys. Rev.* E **55** 5680
[77] Tanaka H and Araki T 2000 *Europhys. Lett.* **51** 154
[78] Toxvaerd S 1999 *Phys. Rev. Lett.* **83** 5318
[79] Bastea S, Puri S and Lebowitz J L 2001 *Phys. Rev.* E **63** 041513
[80] Bastea S and Lebowitz J L 1997 *Phys. Rev. Lett.* **78** 3499
[81] Bird G A 1976 *Molecular Gas Dynamics* (Oxford: Clarendon)
[82] Birdsall C K and Langdon A B 1985 *Plasma Physics via Computer Simulation* (New York: McGraw-Hill)
[83] Cercignani C, Illner R and Pulvirenti M 1994 *The Mathematical Theory of Non-Uniform Gases* (New York: Springer)
[84] Kuksenok O, Yeomans J M and Balazs A C 2002 *Phys. Rev.* E **65** 031502
[85] Kuksenok O and Balazs A C 2003 *Phys. Rev.* E **68** 011502
[86] Fisher M E and Nakanishi H 1981 *J. Chem. Phys.* **75** 5857
Nakanishi H and Fisher M E 1983 *J. Chem. Phys.* **78** 3279
[87] Parry A O and Evans R 1990 *Phys. Rev. Lett.* **64** 439
Parry A O and Evans R 1991 *Phys. Rev. Lett.* **66** 2175
[88] Swift M R, Owczarek A L and Indekeu J O 1991 *Europhys. Lett.* **14** 475
[89] Müller M, Binder K and Albano E V 2001 *Int. J. Mod. Phys.* B **15** 1867
[90] Binder K, Landau D and Müller M 2003 *J. Stat. Phys.* **110** 1411
[91] Aichmayer B, Fratzl P, Puri S and Saller G 2003 *Phys. Rev. Lett.* **91** 015701
[92] Das S K, Puri S, Horbach J and Binder K 2004 in preparation
[93] Toral R and Chakrabarti A 1991 *Phys. Rev.* B **43** 3438
[94] Frisch H L, Puri S and Nielaba P 1999 *J. Chem. Phys.* **110** 10514
[95] Puri S and Frisch H L 1993 *J. Chem. Phys.* **79** 5560
[96] Ince E L 1956 *Ordinary Differential Equations* (New York: Dover)